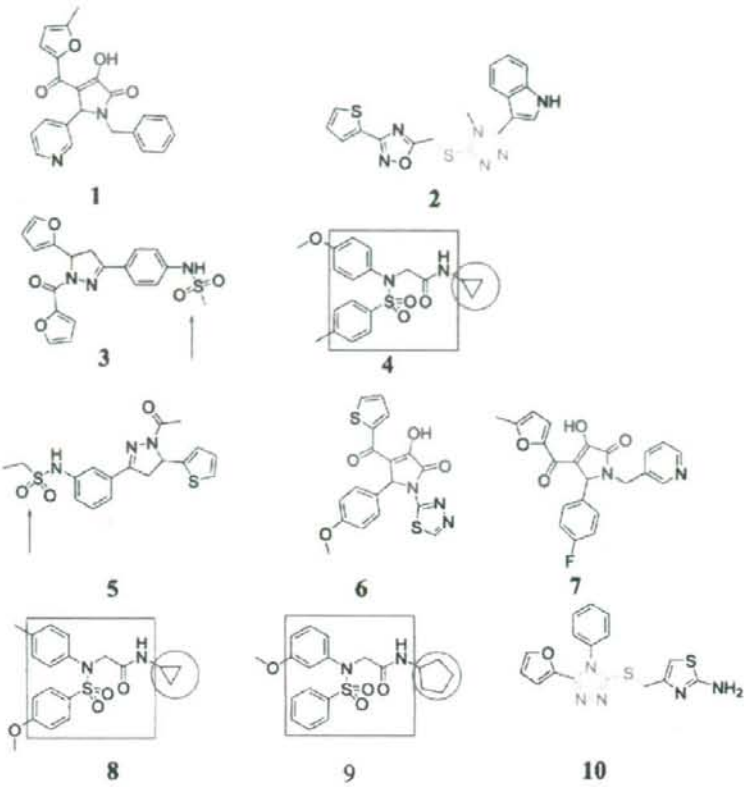

Figure 1. Top 10 ranked compounds identified by DOCK and GOLD screening. Note that there are several shared basic skeletons and functional groups: 1,5-dihydro-2*H*-pyrrol-2-one (drawn in red, compounds **1**, **6**, and **7**), glycinamide (boxed in red, compounds **4**, **8**, and **9**), cycloalkane group (circled in red, compounds **4** and **8**; cyclopropyl, compound **9**; cyclopentyl), 4,5-dihydro-1*H*-pyrazol-3-yl phenyl (drawn in blue, compounds **3** and **5**), sulfonamide (pointed, compounds **3** and **5**), and 4*H*-1,2,4-triazol-3-yl (drawn in green, compounds **2** and **10**).

DOCK–GOLD chained docking screening were tested for their ability to inhibit the hydrolysis activity of UCH-L3, at the Ub-AMC concentration equivalent to the K_m value. Four compounds among these candidates inhibited enzyme activity (Fig. 2a). We did not test the inhibitory effects of compound **3**, as it is a fluorogenic chemical with an emission wavelength of 460 nm. Compounds **1**, **6**, and **7** significantly inhibited the hydrolysis activity of UCH-L3 (initial velocity of Ub-AMC hydrolysis; nM/s [Fig. 2b]). Compounds **1** (401 μM), **6** (375 μM), and **7** (350 μM) inhibited the hydrolysis activity by 83.2 ± 1.5%, 76.5 ± 0.6%, and 76.8 ± 1.0%, respectively, as compared with control DMSO ($p < 0.01$, vs control; Dunnett's test). The IC_{50} value of compound **2** should hypothetically be several hundred μM. Although compound **2** (380 μM) inhibited hydrolysis activity by 16.2 ± 2.1% as compared with control DMSO, the difference was not found to be significant by Dunnett's test. Five other compounds were unable to inhibit the UCH-L3 hydrolysis activity: compound **4** (334 μM; final concentration), compound **5** (331 μM), compound **8** (401 μM), compound **9** (386 μM), and compound **10** (387 μM) (Fig. 2b). Experimentally determined IC_{50} values of compounds **1**, **6**, and **7** (Fig. 3) were as follows: compound **1** (103 μM), compound **6** (154 μM), and compound **7** (123 μM).

2.4. Competitive inhibitor

To show that the identified compounds bind to the active site of the UCH-L3, various concentrations of compound **1** and iodoacetamide (108 mM) were added to UCH-L3/Ub-AMC reaction buffer. Iodoacetamide is a non-competitive inhibitor of UCH-L3 (Fig. 4a). It is a thiol alkylating agent of the UCH-L family and derivatizes and inactivates the active site leading to loss of UCH-L3 enzymatic activity.[22] In the presence of compound 1 and iodoacetamide, the percentage of active UCH-L3 reduced by iodoacetamide treatment was recovered in comparison with the control, and the recovery was dependent on the concentration of compound **1** (Fig. 4b). Our results showed that compound **1** is a competitive inhibitor of UCH-L3. This suggests that compound **1** bound to the UCH-L3 active site to prevent iodoacetamide from inactivating it.

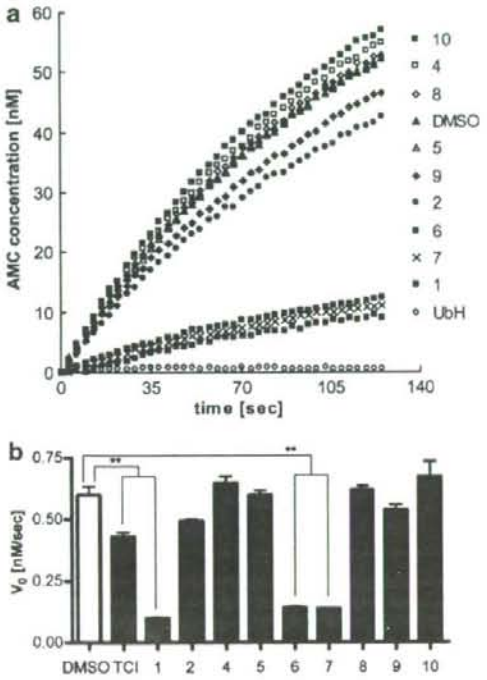

Figure 2. Analysis of UCH-L3 inhibitory effects of compounds 1–10. (a) Kinetics of UCH-L3-catalyzed hydrolysis of Ub-AMC with the compounds. Fluorescence intensity was converted to AMC concentration by subtracting the intensity of fully hydrolyzed substrate from that of solution without substrate. Concentrations of compounds are as follows: compound **1** (401 μM); compound **2** (380 μM); compound **4** (334 μM); compound **5** (331 μM); compound **6** (375 μM); compound **7** (350 μM); compound **8** (401 μM); compound **9** (386 μM); and compound **10** (387 μM). As a known inhibitor, ubiquitin-aldehyde (Ub-H, 120 nM) was used. Each value represents the mean of three independent experiments. (b) Inhibitory effects of compounds on initial velocity of hydrolysis (V_0) are shown. Fluorescence intensity was converted by the same method described in (a). 4,5,6,7-Tetrachloroindan-1,3-dione (TCI, 20 μM) was used as a UCH-L3 selective inhibitor with IC_{50} of 600 nM.[22] Each value represents the mean ± SEM of three independent experiments. Dunnett's multiple comparison test was performed using GraphPad Prism software (**: $p < 0.01$, DMSO as control).[29]

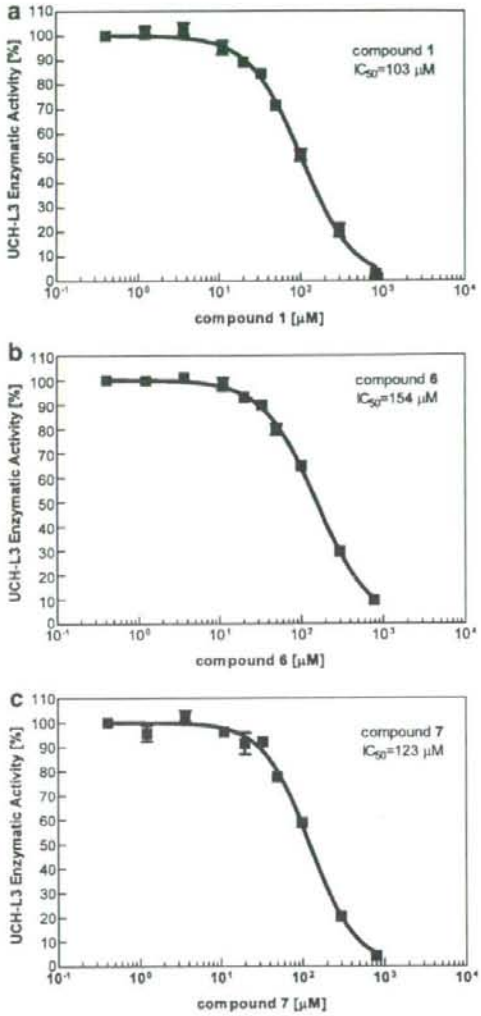

Figure 3. IC_{50} curves of compounds for UCH-L3 enzymatic activity. (a) Compound **1**, (b) compound **6**, and (c) compound **7**. The horizontal axis shows the concentration of each compound. The vertical axis shows the relative UCH-L3 enzymatic activity [%] in comparison with maximal initial velocity. IC_{50} values are shown in graphs. Each plotted value represents the mean ± SEM of three independent experiments.

In order to show that the compounds **1**, **6**, and **7** bind to UCH-L3, Biacore 100 analysis was conducted. Biacore 100 analysis detects interaction between a small molecule and protein and enables quantification of the interaction.[23] The results showed that binding of each compound to UCH-L3 increased and was dependent on the concentration of the compound **6** (data not shown).

2.5. Predicted binding mode

Figure 5 shows the predicted binding modes of compounds **1**, **6**, and **7** to UCH-L3. Since chemical formulae of the three compounds are similar to each other, the predicted docked structures of these and UCH-L3 have similar binding modes. Two hydrogen bonds were observed between the docked ligand and two amino acid residues in the predicted compound **1**/UCH-L3 complex structure; the carbonyl group of compound **1** appears to form a hydrogen bond to the NH group of Ala11, and the pyrrole C=O appears to form a hydrogen bond to the hydroxyl group of Thr157. Three hydrogen bonds were predicted between the docked ligand and two amino acid residues in the compound **6**/UCH-L3 complex structure; the thiadiazole group of compound **6** appears to form a hydrogen bond to the NH group of Leu9, and

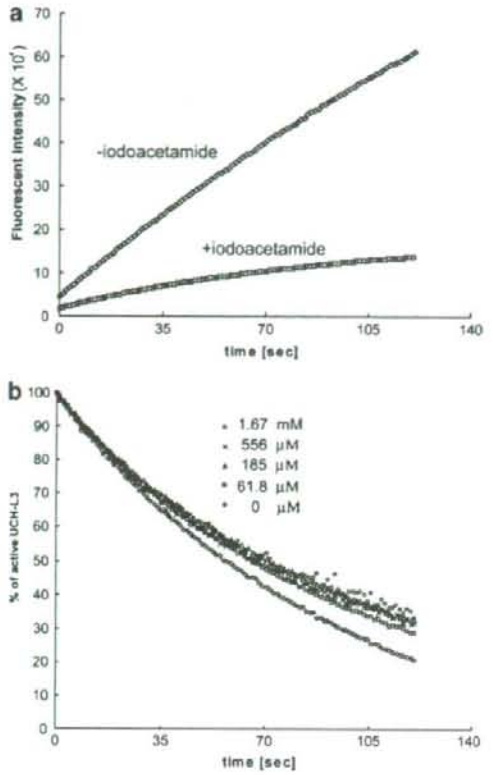

Figure 4. Competitive inhibition of compound 1. (a) Kinetics of UCH-L3-catalyzed hydrolysis of Ub-AMC with or without iodoacetamide (108 mM). (b) Reaction progress curves normalized by final fluorescence intensity representing the ratio of active UCH-L3 (for calculations, see Section 4.9), in the presence of iodoacetamide (108 mM) and compound 1 (0 μM, 61.8 μM, 185 μM, 556 μM, and 1.67 mM).

the pyrrole hydroxyl group and pyrrole C=O appear to form a hydrogen bond to the NH group of Ala11. A hydrogen bond was observed between the docked ligand and the amino acid residues of UCH-L3 in the predicted compound **7**/UCH-L3 complex structure; the carbonyl group of compound **7** appears to form a hydrogen bond to the NH group of Ala11. The predicted binding mode of compound **10**, as a non-binder, was analyzed. Four hydrogen bonds were observed between the docked ligand and the amino acid residues of UCH-L3 in the predicted compound **10**/UCH-L3 complex structure. The triazol group of compound **10** appears to form two hydrogen bonds to the hydroxyl group of Thr157, and the amino group of compound **10** appears to form a hydrogen bond to the CO group of Glu154, and to the CO group of Ser151. Although hydrogen bonds between actual inhibitors (compounds **1**, **6**, and **7**) and Ala11 were observed, compound **10**, a non-inhibitor, does not appear to form a hydrogen bond to Ala11. This hydrogen bond might be important for compounds to bind stably to the UCH-L3 active site.

2.6. Discussion; analysis of active compounds

By three-step virtual screening (DOCK, high-speed GOLD, and low-speed GOLD) of 32,799 chemicals, we identified 10 candidate chemicals that potentially inhibit UCH-L3 hydrolysis activity. We examined the actual inhibitory effects of the compounds on UCH-L3 hydrolysis activity by biochemical enzymatic assay and identified three compounds (compounds **1**, **6**, and **7**) as UCH-L3 inhibitors, with IC_{50} values of 100–150 μM. By comparing the structural formulae of the three compounds, we found that the 1,5-dihydro-2*H*-pyrrol-2-one group is likely to be important for inhibition of UCH-L3-hydrolysis activity (Fig. 6). Several common structural features can be drawn from these three chemicals (Fig. 6). First, the heteroaromatic pyrrole group is common to all three compounds. Second, each of the three compounds also contains pyridines and furoyls as heteroaromatic functional groups. Third, a carbon–oxygen double bond at position 2, a hydroxyl group at position 3, a carbonyl group at position 4, and a hydrogen atom at position 5 of the pyrrole ring are common to each compound. Fourth, a five- or six-membered cyclic group at positions 1, 4, and 5 is common to all three chemicals (Fig. 6). Furthermore, compounds **1** and **7** have two heteroaromatic groups: a pyridinyl group and a furoyl group.

The structural similarities of UCH-L3-binding chemicals have an influence on binding mode similarities. There are two main pockets in the substrate-binding site of UCH-L3: the first pocket (Pocket 1) is formed by Pro8, Glu10, and Thr157 and the second pocket (Pocket 2), the active site pocket, is formed by Asp167, Leu168, and Cys90. Docked orientations of compounds **1** and **7** are very similar, as positions 1 and 5 six-membered cyclic groups fit into each pocket. This suggests that two features among these similarities are likely to be important for stable binding to the active site: a pyrrole ring and two heteroaromatic groups, which fit into both pockets around the UCH-L3 substrate-binding site. The shape of Pocket 1 is different from that of UCH-L1,[24] another isoform of the UCH family (52% amino acid sequence identity).[25] Thus, modification of the chemical groups in Pocket 1 might be effective during drug design, to enhance specificity for UCH-L3 over UCH-L1.

Several lines of evidence indicate that UCH-L3 is associated with tumorigenesis and carcinogenesis. High-level expression and activity of UCH-L3 has been reported in multiple types of cancer cells. Expression of UCH-L3 mRNA is upregulated in breast tumors and UCH-L3 mRNA levels are associated with the histological grading of such tumors.[5] Moreover, it has been suggested that the activity of UCH-L3 is also upregulated in the majority of cervical carcinoma tissues, compared with adjacent normal tissues.[6] On the other hand, loss of UCH-L3 is known to induce cell death in knock-out studies. UCH-L3 is involved in the protection of programmed cell death in germ cells and photoreceptor cells in vivo.[7,8] Thus, the structural information of the

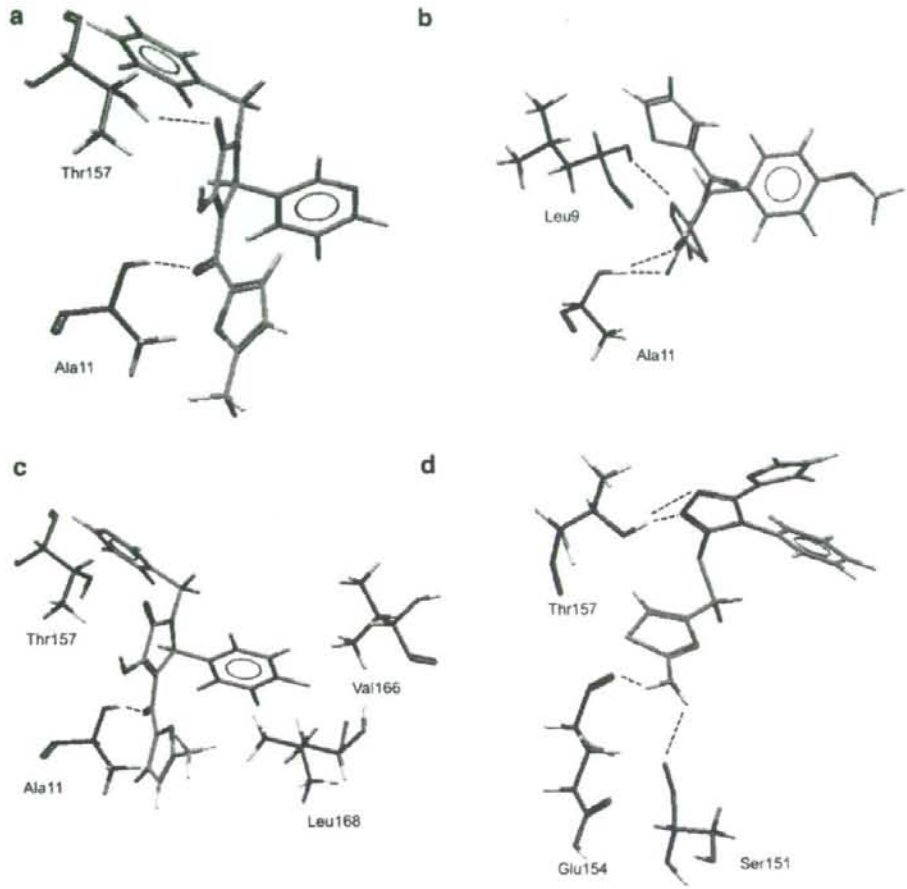

Figure 5. Illustration showing the molecular docking results. Docked orientation of (a) compound **1**, (b) compound **6**, (c) compound **7**, and (d) compound **10** in the UCH-L3 active site using GOLD and shown with interacting residues. Hydrogen bonds are shown by a dashed line. Oxygen atoms are shown in red, nitrogen atoms in blue, sulfur atoms in orange, fluorine atoms in yellow, and hydrogen atoms in gray. The enzyme carbons are shown in dark gray and those of the ligands in green.

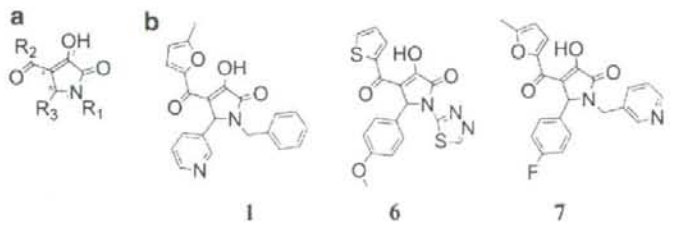

Figure 6. Structural similarities of the three compounds. (a) 1,5-Dihydro-2*H*-pyrrol-2-one group, the common basic skeleton, is shown in red. Position numbers of the pyrrole ring are shown as small characters. R_1–R_3 represent each functional group at positions 1, 4, and 5 of the pyrrole ring, respectively. (b) Structures of identified inhibitors: compounds **1**, **6**, and **7**.

UCH-L3 inhibitors we identified may be useful for future apoptosis-inducing anti-cancer drug development. UCH-L3 should be an important target for modulating cell apoptosis.

3. Conclusion

In this study, we employed three-step docking (DOCK, rough GOLD, and fine GOLD) and in vitro enzyme

assay methods, and identified three UCH-L3 inhibitors with IC_{50} values of 100–150 μM. These novel inhibitors have a dihydro-pyrrole group in common.

4. Experimental

4.1. Compound library

We used the ADME/Tox (absorption, distribution, metabolism, excretion, and toxicity) filtered virtual compound library (ChemBridge CNS-Set) which includes a collection of 32,799 chemical compounds.[18] All compounds satisfy Lipinski's Rule of five.

4.2. Protein preparation

Human UCH-L3 and ubiquitin vinylmethylester (Ub-VME) complex crystal structure data (PDB code; 1XD3) were obtained from Protein Data Bank (PDB).[17] Hydrogens were added to UCH-L3-ubiquitin complex using CVFF99 force field by Biopolymer module in Insight II 2000 suite (Accelrys, Inc., San Diego, CA). Energy was minimized by the Discover 3 module of the same suite with all heavy atoms restrained, except hydrogen, to relieve any short contacts. To use the UCH-L3 protein structure in the following docking simulations, the structures of UCH-L3 and Ub-VME complex were divided into their components.

4.3. Virtual screening

Virtual screening experiments were performed by UCSF DOCK 5.4.0[10] and GOLD 3.0.1 (CCDC, Cambridge, UK).[26] In the first screening by DOCK, the substrate-binding site was defined, by selecting ligand atom accessible spheres and describing molecular surfaces with the SPHERE_GENERATOR program in the DOCK suite. All spheres within 6 Å of root mean square deviation (RMSD) from every atom of the three C-terminal residues of energy-minimized ubiquitin were selected by the SPHERE_SELECTOR program in DOCK suite. A scoring function ($E_{int} = E_{vdw} + E_{elec}$) was used to estimate potential binding affinity. Following the first screening with rigid ligand conditions, 1780 compounds with binding energy scores of less than −30 kcal/mol were selected for a second screening by GOLD.

Using GOLD, the 1780 compounds were screened with 7–8 times speed-up settings; that is, the pre-defined genetic algorithm (GA) parameter settings to achieve calculation speed-up. The top-ranked 100 compounds were determined, then screened by default settings; the GA parameter settings for a slower calculation with greater ligand flexibility, but with a more accurate prediction. Ligand flexibility was turned on in both the 7–8 times speed-up settings and the default settings. Protein side chain flexibility was not turned on in any settings. The virtual tripeptide structure composed of three C-terminal residues of the energy-minimized ubiquitin was set as the reference ligand to define the ligand-binding site. All protein atoms within 5 Å of each ligand atom were used for defining the binding site. The solvent-accessible surfaces of the docking region were restricted by a cavity detection algorithm.[27] As a result, the binding site was composed of 174 active atoms (automatically selected by GOLD software). A method for defining the binding site with tripeptide yielded the best score among other methods using shorter or longer C-terminal peptide sequences of ubiquitin (data not shown). Ten docking solutions for each docked molecule were scored and the top three were saved for post-screening evaluations. Potential hydrogen bonds and van der Waals contacts were identified using Silver 1.0 (CCDC, Cambridge, UK).[28] Ligands predicted to be tight-binders by both DOCK and GOLD were applied to further in vitro experimental validation. All calculations were performed on seven Linux or Cygwin 2–3 GHz/Pentium IV CPU personal computers.

4.4. Statistical analysis

All statistical analysis was performed by GraphPad Prism 4 (GraphPad Software, Inc., San Diego, CA).[29]

4.5. Reagents

Human recombinant UCH-L3, ubiquitin-7-amido-4-methylcoumarin (Ub-AMC), and ubiquitin-aldehyde (Ub-H) were purchased from Boston Biochem, Inc. (Cambridge, MA). 4,5,6,7-Tetrachloroindan-1,3-dione (TCI) was purchased from Fisher Scientific International Inc. (Hampton, NH). Iodoacetamide was purchased from Sigma–Aldrich Corporation (St. Louis, MO). Compounds within ChemBridge CNS-Set (Supplier IDs given in parentheses) are as follows: compound **1**: 1-benzyl-3-hydroxy-4-(5-methyl-2-furoyl)-5-(3-pyridinyl)-1,5-dihydro-2*H*-pyrrol-2-one (7504601); compound **2**: 3-[4-methyl-5-({[3-(2-thienyl)-1,2,4-oxadiazol-5-yl]methyl}thio)-4*H*-1, 2,4-triazol-3-yl]-1*H*-indole (7950509); compound **3**: *N*-{4-[1-(2-furoyl)-5-(2-furyl)-4,5-dihydro-1*H*-pyrazol-3-yl]phenyl}methanesulfonamide (7977303); compound **4**: N^1-cyclopropyl-N^2-(4-methoxyphenyl)-N^2-[(4- methylphenyl)sulfonyl]glycinamide (6382507); compound **5**: *N*-{3-[1-acetyl-5-(2-thienyl)-4,5-dihydro-1*H*-pyrazol-3-yl]phenyl}ethanesulfonamide (7909542); compound **6**: 3-hydroxy-5-(4-methoxyphenyl)-1-(1,3,4-thiadiazol-2-yl)-4-(2-thienylcarbonyl)-1,5-dihydro-2*H*-pyrrol-2-one (6237842); compound **7**: 5-(4-fluorophenyl)-3-hydroxy-4-(5-methyl-2-furoyl)-1-(3-pyridinylmethyl)-1,5-dihydro-2*H*-pyrrol-2-one (6771097); compound **8**: N^1-cyclopropyl-N^2-[(4-methoxyphenyl)sulfonyl]-N^2-(4-methylphenyl)glycinamide (6699002); compound **9**: N^1-cyclopentyl-N^2-(3-methoxyphenyl)-N^2-(phenylsulfonyl)glycinamide (6187162); and compound **10**: 4-({[5-(2-furyl)-4-phenyl-4*H*-1,2,4-triazol-3-yl]thio}methyl)-1,3-thiazol-2-amine (9012750) were purchased from ChemBridge Corporation (San Diego, CA).

4.6. Enzymatic assay

UCH-L3 activity was assayed using modification of a technique described in previous studies.[22,30] The enzyme

reactions were carried out at a final volume of 205 μl on Costar 96-well black assay plates (part number 3915, Corning Inc., Corning, NY). Then, 5 μl of solution containing each compound (100% DMSO), or 5 μl of 100% DMSO as a negative control, was added to 100 μl of enzyme buffer solution (50 pM of UCH-L3, 20 mM Hepes [pH 7.8], 0.5 mM EDTA, 5 mM dithiothreitol [DTT], and 0.1 mg/ml ovalbumin) in each well. The solution was incubated for 30 min at room temperature. To start the enzyme reaction, 100 μl of substrate buffer solution (82 nM of ubiquitin-AMC, 20 mM Hepes [pH 7.8], 0.5 mM EDTA, 5 mM DTT, and 0.1 mg/ml ovalbumin) was added to each well. AMC fluorescence (excitation wavelength: 355 nm, emission wavelength: 460 nm) was subsequently measured 40 times every 3 s with a Wallac 1420 multi-label counter (Perkin-Elmer, Wellesley, MA).

4.7. K_m determination

Fifty microliters of enzyme buffer solution was added to each plate well. The solution was incubated for 30 min at room temperature. To start the enzyme reaction, 50 μl of substrate buffer solution (23.1, 46.3, 92.5, 185, 370, and 740 nM of ubiquitin-AMC; the concentrations of other components were as described previously) was added to each well. Fluorescence of AMC was measured 40 times every 3 s with the Wallac multi-label counter. Initial velocities (from 0 to 30 s) were used for K_m determination, using GraphPad Prism 4 software.[29]

4.8. Experimental IC_{50} determination

Five microliters of solution containing each compound (0.412 μM, 1.23, 3.70, 11.1, 20, 33.3, 50, 100, 300, and 700–850 μM) or 5 μl of 100% DMSO (as a negative control) diluted in 100 μl of enzyme buffer solution was added to each plate well. This solution was incubated for 30 min at room temperature. To start the enzyme reaction, 100 μl of substrate buffer solution was added to each well. Fluorescence of AMC was measured 40 times every 3 s with the Wallac multi-label counter. Initial velocities (from 0 to 30 s) were used for IC_{50} determination, using GraphPad Prism 4 software.[29]

4.9. Active site binding experiment

Modification of a technique described in previous studies was used to determine whether or not the compounds bind to the active site.[22] Five microliters of solution containing compound **1** (0 μM, 61.8 μM, 185 μM, 556 μM, and 1.67 mM) or 5 μl of 100% DMSO (as a negative control) diluted in 80 μl of enzyme buffer solution (UCH-L3: 1 nM) was added to each plate well. This solution was incubated for 30 min at room temperature. To start the enzyme reaction, 80 μl of substrate buffer solution (Ub-AMC: 1 μM) was added to each well, followed within 2 s by addition of 40 μl of iodoacetamide (108 mM) or water as a negative control. Fluorescence of AMC was measured 100 times every second using the Wallac multi-label counter. The percentage of active site survival $[(F_{saturated} - F_t)/(F_{saturated} - F_{t=0}) \times 100]$ was calculated.

Acknowledgments

This work was supported by Grants-in-Aid for Scientific Research from the Ministry of Health, Labour and Welfare of Japan, Grants-in-Aid for Scientific Research from the Ministry of Education, Culture, Sports, Science and Technology of Japan, a grant from the Program for Promotion of Fundamental Studies in Health Sciences of the National Institute of Biomedical Innovation, a grant from Japan Science and Technology Cooperation, and a grant from New Energy and Industrial Technology Development Organization. We thank Takashi Kaburagi for demonstrating how to set up the DOCK software.

References and notes

1. Ciechanover, A.; Schwartz, A. L. *Proc. Natl. Acad. Sci. U.S.A.* **1998**, *95*, 2727–2730.
2. Pickart, C. M.; Rose, I. A. *J. Biol. Chem.* **1985**, *260*, 7903–7910.
3. Waldmeier, P.; Bozyczko-Coyne, D.; Williams, M.; Vaught, J. L. *Biochem. Pharmacol.* **2006**, *72*, 1197–1206.
4. Aktas, O.; Waiczies, S.; Zipp, F. *J. Neuroimmunol.* **2007**, *184*, 17–26.
5. Miyoshi, Y.; Nakayama, S.; Torikoshi, Y.; Tanaka, S.; Ishihara, H.; Taguchi, T.; Tamaki, Y.; Noguchi, S. *Cancer Sci.* **2006**, *97*, 523–529.
6. Rolen, U.; Kobzeva, V.; Gasparjan, N.; Ovaa, H.; Winberg, G.; Kisseljov, F.; Masucci, M. G. *Mol. Carcinog.* **2006**, *45*, 260–269.
7. Kwon, J.; Wang, Y. L.; Setsuie, R.; Sekiguchi, S.; Sato, Y.; Sakurai, M.; Noda, M.; Aoki, S.; Yoshikawa, Y.; Wada, K. *Am. J. Pathol.* **2004**, *165*, 1367–1374.
8. Sano, Y.; Furuta, A.; Setsuie, R.; Kikuchi, H.; Wang, Y. L.; Sakurai, M.; Kwon, J.; Noda, M.; Wada, K. *Am. J. Pathol.* **2006**, *169*, 132–141.
9. Kuntz, I. D.; Blaney, J. M.; Oatley, S. J.; Langridge, R.; Ferrin, T. E. *J. Mol. Biol.* **1982**, *161*, 269–288.
10. Ewing, T. J.; Makino, S.; Skillman, A. G.; Kuntz, I. D. *J. Comput. Aided Mol. Des.* **2001**, *15*, 411–428.
11. FlexX, BioSolveIT GmbH, Sankt Augustin, Germany, <http://www.biosolveit.de/>.
12. Peng, H.; Huang, N.; Qi, J.; Xie, P.; Xu, C.; Wang, J.; Yang, C. *Bioorg. Med. Chem. Lett.* **2003**, *13*, 3693–3699.
13. McNally, V. A.; Gbaj, A.; Douglas, K. T.; Stratford, I. J.; Jaffar, M.; Freeman, S.; Bryce, R. A. *Bioorg. Med. Chem. Lett.* **2003**, *13*, 3705–3709.
14. Olsen, L.; Jost, S.; Adolph, H. W.; Pettersson, I.; Hemmingsen, L.; Jorgensen, F. S. *Bioorg. Med. Chem.* **2006**, *14*, 2627–2635.
15. Miteva, M. A.; Lee, W. H.; Montes, M. O.; Villoutreix, B. O. *J. Med. Chem.* **2005**, *48*, 6012–6022.
16. Johnston, S. C.; Larsen, C. N.; Cook, W. J.; Wilkinson, K. D.; Hill, C. P. *EMBO J.* **1997**, *16*, 3787–3796.
17. Misaghi, S.; Galardy, P. J.; Meester, W. J.; Ovaa, H.; Ploegh, H. L.; Gaudet, R. *J. Biol. Chem.* **2005**, *280*, 1512–1520.
18. RPBS, Paris, France, <http://bioserv.rpbs.jussieu.fr/RPBS/cgi-bin/Ressource.cgi?chzn_lg=an&chzn_rsrc=Collections/>.
19. GOLD User Guide, 16.2.1, CCDC, Cambridge, UK, <http://www.ccdc.cam.ac.uk/support/documentation/gold/3_1/gold31.pdf/>.
20. Dang, L. C.; Melandri, F. D.; Stein, R. L. *Biochemistry* **1998**, *37*, 1868–1879.

21. Mason, D. E.; Ek, J.; Peters, E. C.; Harris, J. L. *Biochemistry* **2004**, *43*, 6535–6544.
22. Liu, Y.; Lashuel, H. A.; Choi, S.; Xing, X.; Case, A.; Ni, J.; Yeh, L. A.; Cuny, G. D.; Stein, R. L.; Lansbury, P. T., Jr. *Chem. Biol.* **2003**, *10*, 837–846.
23. Stenlund, P.; Frostell-Karlsson, A.; Karlsson, O. P. *Anal. Biochem.* **2006**, *353*, 217–225.
24. Das, C.; Hoang, Q. Q.; Kreinbring, C. A.; Luchansky, S. J.; Meray, R. K.; Ray, S. S.; Lansbury, P. T.; Ringe, D.; Petsko, G. A. *Proc. Natl. Acad. Sci. U.S.A.* **2006**, *103*, 4675–4680.
25. Kurihara, L. J.; Semenova, E.; Levorse, J. M.; Tilghman, S. M. *Mol. Cell. Biol.* **2000**, *20*, 2498–2504.
26. Jones, G.; Willett, P.; Glen, R. C.; Leach, A. R.; Taylor, R. *J. Mol. Biol.* **1997**, *267*, 727–748.
27. Hendlich, M.; Rippmann, F.; Barnickel, G. *J. Mol. Graph. Model.* **1997**, *15*, 359–363.
28. Silver, CCDC, Cambridge, UK, <http://www.ccdc.cam.ac.uk/>.
29. GraphPad Prism 4, GraphPad Software, San Diego, CA, <http://www.graphpad.com/www/about.htm/>.
30. Nishikawa, K.; Li, H.; Kawamura, R.; Osaka, H.; Wang, Y. L.; Hara, Y.; Hirokawa, T.; Manago, Y.; Amano, T.; Noda, M.; Aoki, S.; Wada, K. *Biochem. Biophys. Res. Commun.* **2003**, *304*, 176–183.

3, respectively). To determine whether the difference in locomotor activity on day 1 was due to reduced exploratory behaviour in *gad* mice, we measured the frequency of rearing, a typical exploratory behaviour (Lever *et al.*, 2006; Fig. 2E). Similar to locomotor activity, upon re-exposure rearing frequency decreased in wild-type mice ($P = 0.009$, $F = 14.257$, $n = 7$; repeated-measures ANOVA) but not in *gad* mice ($P = 0.131$, $F = 2.503$, $n = 6$; repeated-measures ANOVA). The rearing frequency on days 1 and 2 differed significantly between wild-type and *gad* mice ($P = 0.014$ and 0.021 for days 1 and 2, respectively; two-tailed Student's *t*-test), but the activity on day 3 did not ($P = 0.093$). These results suggest that exploratory behaviour in a novel environment is reduced in *gad* mice.

Although these data apparently suggest that memory in passive avoidance learning and exploratory behaviour are reduced in young *gad* mice, there is a possibility that the anxiety state of *gad* mice is altered. Alterations in the anxiety state can affect memory (Bouton *et al.*, 1990) and the response to novel environments. To measure anxiety, we performed a light–dark box test. In this test, mice usually avoid the light compartment. Therefore, the level of anxiety can be measured as the latency to move into the light compartment and the duration of time in the light compartment (Yamada *et al.*, 2002). Because the passive avoidance test also utilizes these properties, performance in the light–dark test is important for interpreting the results from the passive avoidance test. The time required for the mice to step into the light compartment when introduced into the dark compartment (dark-light latency; Fig. 3A), the time the mice spent in the light compartment (Fig. 3A) and the number of times the mice crossed between compartments (Fig. 3B) did not differ significantly between wild-type and *gad* mice ($P = 0.834$, 0.417 and 0.109, respectively; two-tailed Student's *t*-test). These results suggest that anxiety state, as assessed by this test, was not obviously altered in *gad* mice. Therefore we concluded that the impairments in passive avoidance learning and exploratory behaviour were not due to alterations in the anxiety state.

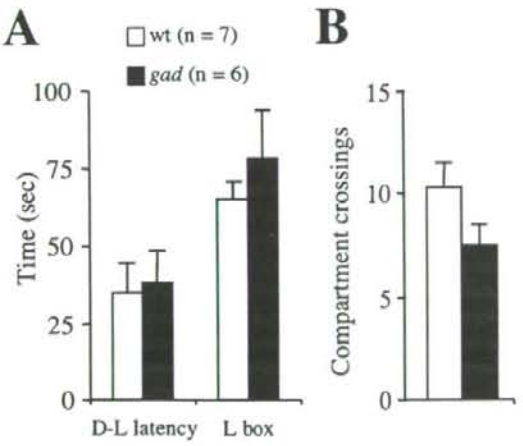

FIG. 3. Wild-type and *gad* mice performed similarly in the light–dark box test. (A) Dark–light (D-L) latency and duration of time in the light compartment (L box). (B) Number of crossings between the two compartments.

Impairment of a transcription-dependent component of LTP in gad mice

We tested whether the lack of UCH-L1 affects neuronal function by measuring LTP at Schaffer collateral synapses onto CA1 pyramidal neurons in hippocampal slice preparations. LTP is believed to be a synaptic mechanism underlying memory and learning (Bliss & Collingridge, 1993). The CA1 synapse was selected because this brain region is involved in spatial memory (Morris *et al.*, 1982) and passive avoidance memory (Bevilaqua *et al.*, 1997; Impey *et al.*, 1998). In wild-type slices, TBS induced robust LTP at CA1 synapses (Fig. 4A), as reported for C57BL/6J mice (Nguyen & Kandel, 1997; Nguyen *et al.*, 2000). In contrast, TBS-induced LTP was attenuated in *gad* mice beginning ~20 min post-TBS (Fig. 4A). At 45 min post-TBS, normalized synaptic responses were significantly greater in wild-type slices (1.87 ± 0.08, $n = 7$) than in *gad* slices (1.36 ± 0.07, $n = 6$; $P = 0.001$, two-tailed Student's *t*-test). Impairment of LTP in *gad* mice depended on the stimulation pattern. Tetanus-induced LTP was identical in wild-type and *gad* mice (Fig. 4B; normalized fEPSP slopes at 45 min post-tetanus: wild-type, 1.81 ± 0.16, $n = 5$; *gad*, 1.86 ± 0.25, $n = 5$).

Stimulus–output curves (Fig. 5A) and paired-pulse facilitation (Fig. 5B) of CA1 synapses were essentially identical in wild-type and *gad* mice. The latter result suggests that a postsynaptic, rather than presynaptic, mechanism is involved in impairment of TBS-induced LTP in *gad* mice. LTP at this synapse is dependent on postsynaptic NMDA receptors (Harris *et al.*, 1984; Larson & Lynch, 1988). Therefore, we tested whether NMDA receptor activity was reduced in *gad* mice using patch-clamp recordings. For this purpose, we recorded Schaffer collateral–CA1 synaptic responses in neurons voltage-clamped to −70 and +40 mV in the presence of picrotoxin (50 μM). The amplitude of the synaptic response recorded at +40 mV at 100 ms poststimulation was normalized to the peak amplitude of the response at −70 mV to estimate the ratio of NMDA-mediated to non-NMDA-mediated currents (Fig. 5D). Because superfusion of the slices with picrotoxin frequently elicited epileptiform activity (data not shown), three to five synaptic responses without epileptiform activity were selected and averaged. The ratio was identical in wild-type and *gad* mice (0.45 ± 0.05, $n = 5$ and 0.43 ± 0.05, $n = 7$ for wild-type and *gad* mice, respectively; two-tailed Student's *t*-test). Therefore, attenuation of synaptic NMDA receptor activity does not account for reduced LTP in *gad* mice. Resting membrane potential and input resistance of CA1 pyramidal neurons did not differ substantially between wild-type and *gad* mice [resting membrane potential, -60.1 ± 0.4 mV for wild-type mice ($n = 20$) and -60.0 ± 0.6 mV for *gad* mice ($n = 20$); input resistance, 163 ± 9.6 for wild-type mice ($n = 16$) and 175 ± 10.8 for *gad* mice ($n = 13$); results obtained from the records using potassium-gluconate pipette solution].

CA1 LTP is composed of early and late temporal phases (Nguyen *et al.*, 1994; Abel *et al.*, 1997; Nguyen & Kandel, 1997). The former is induced mainly by an increase in the number of AMPA-type glutamate receptors at the synapse (reviewed in Malinow & Malenka, 2002) whereas the latter is induced by new protein synthesis from transcription of new mRNA (Nguyen *et al.*, 1994) and/or local protein synthesis from previously expressed mRNA (Bradshaw *et al.*, 2003). Because no obvious changes in the early phase of LTP (up to ~20 min post-TBS) were observed in *gad* mice, we tested whether the late phase is occluded in *gad* mice. For this purpose, we applied actinomycin D, a transcription inhibitor, to the slices and compared suppression of TBS-induced LTP in wild-type and *gad* mice. In wild-type mice, the maintenance of TBS-induced LTP was suppressed by actinomycin D (Fig. 6A). The normalized fEPSP slope at 45 min

Available online at www.sciencedirect.com
ScienceDirect
European Journal of Pharmacology 573 (2007) 20–28
www.elsevier.com/locate/ejphar

Alpha 1-adrenoceptor agonists protect against stress-induced death of neural progenitor cells

Hiroki Ohashi [a,b], Kaori Nishikawa [a,c], Koichi Ayukawa [a,d], Yoko Hara [a], Mika Nishimoto [a,e], Yoshihisa Kudo [e], Toshiaki Abe [b], Shunsuke Aoki [a,c,f,*], Keiji Wada [a,f]

[a] Department of Degenerative Neurological Diseases, National Institute of Neuroscience, NCNP, Kodaira, Tokyo 187-8502, Japan
[b] Department of Neurosurgery, Jikei University Graduate School of Medicine, Minatoku, Tokyo 105-8401, Japan
[c] NEDO (New Energy and Industrial Technology Development Organization), Kawasaki, Kanagawa 212-8554, Japan
[d] Japan Society for the Promotion of Science (JSPS), Chiyodaku, Tokyo 102-8471, Japan
[e] Laboratory of Cellular Neurobiology, Tokyo University of Pharmacy and Life Science, Hachioji, Tokyo 192-0392, Japan
[f] CREST (Core Research for Evolutional Science and Technology) of Japan Science and Technology Corporation (JST), Kawaguchi, Saitama 332-0012, Japan

Received 15 February 2007; received in revised form 18 June 2007; accepted 26 June 2007
Available online 12 July 2007

Abstract

Here, we show that α_1-adrenoceptor agonists suppress stress-induced death of mouse embryonic brain-derived neural progenitor cells (NPCs). NPCs highly expressed both α_{1A}- and α_{1B}-adrenoceptor genes, whereas the gene encoding α_{1D}-adrenoceptor was expressed at low levels. Application of the α_1-adrenoceptor agonists phenylephrine and cirazoline significantly promoted cell survival of embryonic NPCs that had been exposed to stress, as measured by a lactate dehydrogenase release assay, but had no remarkable effect on differentiation of the NPCs. Both phenylephrine and cirazoline protected NPCs from death induced by growth factor deprivation, N2 nutrient deprivation, tunicamycin treatment or staurosporine treatment. Phenylephrine and cirazoline treatments both maximally reduced stress-induced cell death by ~60% but did not change the percentage of undifferentiated cells as measured by nestin staining. Moreover, phenylephrine and cirazoline treatments did not affect the cellular activities of caspase-3 and caspase-7 but markedly reduced propidium iodide penetration into the cytoplasm, suggesting that α_1-adrenoceptor agonists inhibit caspase-3/7-independent death of the embryonic NPCs.

Keywords: α_1-adrenoceptor; GPCR; Neural progenitor cell; Cell death; Cell stress; Phenylephrine; Cirazoline

1. Introduction

The noradrenergic system is proposed to play multiple roles in the adult central nervous system (CNS). Apart from its classical transmitter signaling action, noradrenaline has important roles in attention, arousal, and memory reviewed in Murchison et al., (2004); Southwick et al., (1999). Furthermore, it was proposed that noradrenaline influences the survival, maintenance and plasticity of CNS neurons, including the regulation of endogenous neurotrophin systems, glial function, CNS energy utilization and extracellular homeostasis, and has anti-inflammatory and anti-oxidant effects reviewed in Marien et al., (2004). All cell surface adrenoceptors are members of the G protein-coupled receptor family and mediate responses to extracellular noradrenaline. To date, three subfamilies of adrenoceptors (α_1, α_2 and β) have been identified (Bylund et al., 1995). The adrenoceptors are expressed in many tissues, particularly in the cardiovascular, genitourinary and nervous systems. High levels of adrenoceptors are also present in the neocortex during embryogenesis (Lidow and Rakic, 1992), and there are regional concentrations of α_1, α_2, and β adrenoceptors in the fetal forebrain (Lidow and Rakic, 1994). There are three subtypes of α_1-adrenoceptors, the α_{1A}, α_{1B}, α_{1D}-adrenoceptor, with varying degrees of efficiency of G protein (Gq/11) coupling ($\alpha_{1A}>\alpha_{1B}>\alpha_{1D}$ adrenoceptor) reviewed in Hieble et al., (1995). This leads to activation of downstream signal

* Corresponding author. Department of Degenerative Neurological Diseases, National Institute of Neuroscience, National Center of Neurology and Psychiatry, 4-1-1 Ogawahigashi, Kodaira, Tokyo 187-8502, Japan. Tel.: +81 42 346 1715; fax: +81 42 346 1745.
E-mail address: aokis@ncnp.go.jp (S. Aoki).

0014-2999/$ - see front matter © 2007 Elsevier B.V. All rights reserved.
doi:10.1016/j.ejphar.2007.06.060

transduction pathways, including Ca^{2+}, arachidonic acid, phospholipase C and phospholipase D signals reviewed in Zhong and Minneman (1999). α_1-adrenoceptors are specifically localized to NPCs located in the ventricular zone and subventricular zone in the embryonic rat forebrain, and noradrenaline-containing fibers are also present in both the ventricular zone and subventricular zone (Pabbathi et al., 1997). In addition, noradrenaline has been suggested to regulate development of the murine forebrain. The β-adrenoceptor agonist isoproterenol alters proliferation and differentiation of neural precursors in the cerebral cortex (Slotkin et al., 1988). α_1-adrenoceptors were also implicated in controlling cell proliferation and survival in a rat cortical mixed cell culture and in a heterochronic coculture system of the rat neocortex and rostral pons (Pabbathi et al., 1997; Popovik and Haynes, 2000). Although the functions of α_1-adrenoceptors in the mixed-culture NPCs and in the organ culture were investigated, the function of α_1-adrenoceptors and the direct effects of α_1-adrenoceptor-selective agonists such as phenylephrine and cirazoline in isolated pure embryonic NPCs are not known.

The precise role of the α_1-adrenoceptor-mediated signal in embryonic cortical NPCs remains obscure, because the effects observed in the mixed-cell and organ culture experiments possibly reflect the secondary and tertiary effects mediated by multiple cellular interactions (glial cell-progenitor, neuronal cell-progenitor and neuronal cell-glial cell-progenitor interactions). As such, the aim of this study is to know the primary biological effect of α_1-adrenoceptor activation in the NPCs. We addressed the biological effects of α_1-adrenoceptor-selective agonists on highly purified embryonic NPCs. Our data indicate that these agonists inhibit death of NPCs cultured under various stress conditions but do not affect proliferation, differentiation or caspase-3/7-activity.

2. Materials and methods

2.1. Animals

Pregnant C57BL/6J mice were purchased from CLEA Japan (Tokyo, Japan). Animal care and handling were in accordance with institutional regulations for animal care and public law, and were approved by the Animal Investigation Committee of the National Institute of Neuroscience, Japan.

2.2. Antibodies and reagents

Monoclonal and polyclonal antibodies used in this study were as follows: monoclonal anti-nestin (Becton Dickinson, Lexington, KY), monoclonal anti-tuj1 (Covance, Berkeley, CA), polyclonal anti-glial fibrillary acidic protein (Dako, Carpinteria, CA), monoclonal anti-galactocerebroside (Chemicon International, Temecula, CA). The secondary antibodies conjugated to Alexa Fluor dye were purchased from Molecular Probes (Eugene, OR). α_1-adrenoceptor agonists used in this study were (*R*)-3-[1-hydroxy-2-(methylamino) ethyl] phenol (phenylephrine; Sigma, St. Louis, MO) and 2-[(2-cyclopropyl-phenoxy) methyl]-4, 5-dihydro-1H-imidazole (cirazoline; Tocris, Ellisville, MO). Each agonist was dissolved in Neurobasal™ medium (Invitrogen, Carlsbad, CA). Staurosporine and tunicamycin (Sigma) were dissolved in dimethyl sulfoxide (DMSO). Each solution was added to the medium, and the final concentration of DMSO in the medium was adjusted to at most 0.1% (v/v). Medium containing the same amount of organic solvent was used as a negative control.

2.3. Cortical NPCs culture

Cortical NPCs were cultured as previously described (Fukazawa et al., 2006). Briefly, embryos were removed from pregnant C57BL/6J mice and were staged according to morphological criteria to confirm gestational age. Developing mouse brain and cerebral cortex containing the ventricular and subventricular zones were dissected from embryonic day 14 (E14) embryos. Cells were mechanically dissociated by trituration and plated at 3.0×10^6 cells per 10-cm dish (BD) precoated with 15 μg/ml poly-L-ornithine (Sigma) and 1 μg/ml fibronectin (Nitta Gelatin, Osaka, Japan). Cells were expanded for 4 days in serum-free Neurobasal medium supplemented with 0.5 mM L-glutamine (Invitrogen), 100 U/ml penicillin, 100 μg/ml streptomycin (Invitrogen) and B27 (biotin, L-carnitine, corticosterone, ethanolamine, D(+)-galactose, glutathione (reduced), linoleic acid, linolenic acid, progesterone, putrescine, retinyl acetate, selenium, T3 (triodo-l-thyronine), DL-α-tocopherol (vitamin E), DL-α-tocopherol acetate, bovine serum albumin, catalase, insulin, superoxide dismutase, transferrin, vitamin A (Brewer et al., 1993); Invitrogen). N2 supplement (100 mg/l apo-transferrin, 5 mg/l insulin, 16 mg/l putrescine, 6.3 μg/l progesterone, 5 μg/l selenite; Sigma) were used for stress experiments instead of the B27 supplement. This medium was supplemented with 10 ng/ml basic fibroblast growth factor (bFGF; PeproTech, Rocky Hill, NJ) except when mentioned otherwise. Cultures were maintained at 37 °C in an atmosphere of 95% air and 5% CO_2. For secondary cultures, bFGF-expanded cortical NPCs were washed in warm Hanks' balanced salt solution, detached with mechanically pipetting, and resuspended in Neurobasal medium. Cells were then re-seeded on 24-well plates (Nunc; 1.8×10^5 cells/well), or 48-well plates (Nunc; 1.5×10^5 cells/well) precoated with poly-L-ornithine and fibronectin.

2.4. Real-time quantitative reverse-transcription (RT)-PCR

Real-time quantitative RT-PCR with the SYBR Green-based detection method was performed as previously described (Aoki et al., 2002). Total RNA was isolated from cultured cortical NPCs and E14 mouse cerebral cortex. These RNAs (1 μg) were treated with DNase I and converted to cDNA with Superscript II reverse transcriptase (Invitrogen) and random hexamer primers according to the manufacturer's instructions. The efficiency of reverse transcription and the quality of cDNA was compared with the efficiency of PCR amplification of the hypoxanthine guanine phosphoribosyl transferase (hprt) gene (GenBank accession ID. NM_013556; forward primer, 5′-TCTTTGCTGACCTGCTG-GATT-3′; reverse primer, 5′-TATGTCCCCCGTTGACTGATC-

3′). Primers were designed for the α_{1A} (NM_013461), α_{1B} (NM_007416) and α_{1D} (NM_013460) adrenoceptor genes using Primer Express software (Perkin-Elmer, Torrance, CA). The forward and reverse primer sequences were as follows: 5′-TTTCAAGCCACCGGAAACA-3′ and 5′-ACTGGATTCGCAGCACATTCT-3′ (α_{1A}); 5′-AACCCTTCTACGCCCTCTTTTC-3′ and 5′-CCAGATTCTTGGTGGTCCTCTT-3′ (α_{1B}); and 5′-TCGCTCAAGTATCCAGCCATT-3′ and 5′-AACCTAGTAGCGGTCCCACAGA-3′ (α_{1D}). SYBR Green-based real-time RT-PCR was performed in 12.5-μl reactions (ABI PRISM 7700 Sequence Detection System, Perkin-Elmer). PCR products were analyzed with agarose gel electrophoresis. We checked each primer individually to ensure that the primer was selective for the target (data not shown). We also ensured that no band was observed in gel electrophoresis of PCRs that included distilled water or total RNA preparation without reverse transcriptase as template. The quantitative RT-PCR method (User Bulletin #2, Applied Biosystems, Foster City, CA) was modified to establish an expression level index for mRNA (Aoki et al., 2002), and the SYBR Green signal for the hprt amplicon was used as a reference. Amplification efficiency was determined and confirmed in a control PCR experiment using serial cDNA dilutions as templates. The real-time RT-PCR products were analyzed using the Applied Biosystems sequence detection system software 1.7.

2.5. LDH and ATP assay

The number of non-viable cortical NPCs was quantitatively assayed by measuring the activity of the cytosolic enzyme lactate dehydrogenase (LDH) released into the culture medium after membrane rupture. LDH activity was measured using the cytotoxicity assay CytoTox-ONE™ Homogeneous Membrane Integrity Assay (Promega, Madison, WI). To quantify the number of viable cells in cultured cortical NPCs, the amount of cellular ATP was measured using the CellTiter-Glo™ Luminescent Cell Viability Assay (Promega). These assays were performed in accordance with the manufacturer's protocol and on secondary cultured cortical NPCs as described above. Four hundred μl (1.5×10^5 cells/well) of cell suspension was added to each well of a 48-well plate (Nunc) precoated with poly-L-ornithine and fibronectin. After 24 h, cells were treated without or with 10 μM phenylephrine or cirazoline with different concentrations of bFGF or under different stress conditions as described in the figure legends. Cultures were then returned to the 37 °C incubator for 24 h, and assessment of LDH release in the media and amount of ATP was conducted with a Wallac 1420 multilabel counter (Perkin-Elmer, Finland).

2.6. Immunocytochemistry

Cells were stained as we have previously described with minor modifications (Sakurai et al., 2006). Briefly, all incubations and washes were performed at room temperature. Cells were fixed with 3.8% formaldehyde in phosphate-buffered saline (PBS) for 10 min and permeabilized with 0.02% (w/v) Triton X-100 in PBS for 5 min. Fixed cells were blocked with 3.3% goat serum in PBS for 30 min. Cells were incubated for 30 min with anti-nestin (neural progenitor marker; 1:500), anti-tuj1 (early neuronal cell marker; 1:500)(Sakurai et al., 2006), anti-glial fibrillary acidic protein (astrocyte marker; 1:1000) or anti-galactocerebroside (immature oligodendrocyte marker; 1:200)(Fukazawa et al., 2006). These cells were incubated with diluted secondary antibody (1:200) conjugated to Alexa Fluor for 30 min. All primary and secondary antibodies were diluted in 1% goat serum in PBS before use. The fluorescence microscopy images were obtained with an IX70 microscope (Olympus).

2.7. Quantification of enzymatic activities of caspases

Caspase-3 and caspase-7 protease activities were determined using the Caspase-Glo™ 3/7 Assay kit (Promega). All assays were performed on secondary cultured cortical NPCs as described above. Four hundred μl (1.5×10^5 cells/well) of cell suspension was added to each well of a 48-well plate (Nunc) precoated with poly-L-ornithine and fibronectin. After 24 h, cells were treated with or without 10 μM phenylephrine in medium lacking the N2 supplement as described in the figure legends. Cultures were then returned to the 37 °C incubator for 24 h, and caspase-3 and -7 activities were assessed with a Wallac 1420 multilabel counter.

2.8. Measurement of cell death using propidium iodide

All assays were performed on secondary cultured cortical NPCs as described above. Four hundred μl (1.5×10^5 cells/well) of cell suspension was added to each well of a 48-well plate (Nunc) precoated with poly-L-ornithine and fibronectin. After 24 h, cells were treated with or without 10 μM phenylephrine in medium lacking the N2 supplement. Cultures were then returned to the 37 °C incubator and maintained for 24 h, then stained with 1 μg/ml propidium iodide. Only dead cells with permeable plasma membranes were stained with propidium iodide. Positive controls were stained with propidium iodide after fixing with 3.8% formaldehyde in PBS for 10 min and permeabilized with 0.02% Triton X-100 in PBS. Dead cells and positive controls stained with propidium iodide were counted by fluorometry (Wallac 1420 multilabel counter).

2.9. Statistical analysis

Results are expressed as the mean ± standard error of the mean (S.E.M.). Either the Student's *t*-test or Dunnett's multiple range test was used to evaluate the data using Prism software version 4.03 (GraphPad, San Diego, CA). Values of $P<0.01$ and $P<0.05$ were considered statistically significant depending on the specific experiment.

3. Results

3.1. Embryonic cortical NPCs express α_1-adrenoceptor genes

We analyzed gene expression levels of the three α_1-adrenoceptors, and all were expressed both in the E14 embryonic

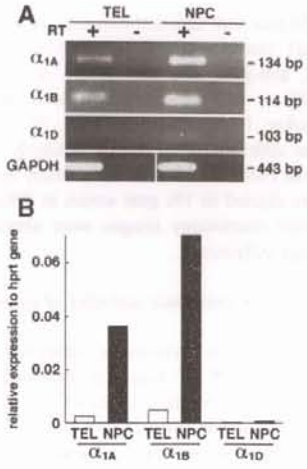

Fig. 1. NPCs derived from E14 telencephalon express α_{1A}-adrenoceptor (α_{1A}), α_{1B}-adrenoceptor (α_{1B}) and α_{1D}-adrenoceptor (α_{1D}). Total RNA isolated from cultured NPCs and E14 mouse telencephalon (TEL) was reverse-transcribed, and the resultant cDNA was used in RT-PCR analysis. (A) As indicated on the left, the PCR products corresponding to the α_{1A}, α_{1B}, and α_{1D} adrenoceptor genes and *GAPDH* were separated on a 3% agarose gel. The size of PCR products are indicated on the right. (B) Gene expression levels of the α_{1A}, α_{1B} and α_{1D} adrenoceptor were analyzed by quantitative RT-PCR, and the expression levels relative to *hprt* are presented. The results are representative of three separate experiments that yielded similar results.

telencephalon and E14 telencephalon-derived cultured NPCs (Fig. 1A). Semi-quantitative analysis of expression levels of the α_1-adrenoceptor genes (normalized to the internal control, *hprt*) showed that the isolated NPCs highly expressed α_{1A}, α_{1B} and α_{1D} adrenoceptor genes as compared with the E14 telencephalon (Fig. 1B). Among the α_1-adrenoceptor genes, the α_{1A} and α_{1B} genes were highly expressed in the cultured NPCs, whereas a low level of expression was detected for the α_{1D} gene in both the E14 telencephalon and cultured NPCs (Fig. 1B).

3.2. Effect of the α_1-adrenoceptor agonist phenylephrine on NPC differentiation

E14 telencephalon-derived NPCs have potencies to differentiate into multiple neural cell types, including neurons, astrocytes and oligodendrocytes, in the absence of bFGF (Fig. 2). The effect of phenylephrine, an α_1-adrenoceptor-selective agonist, on NPC differentiation was examined using the neural cell differentiation marker tuj1 for neuronal cells, glial fibrillary acidic protein for astroglial cells and galactocerebroside for oligodendrocytes. At 72 h after bFGF deprivation, 41.8±1.0% of the NPCs had differentiated into tuj1-positive (tuj1$^+$) cells, 40.6±6.0% of the NPCs had differentiated into glial fibrillary acidic protein-positive (GFAP$^+$) cells and 9.4±1.1% were galactocerebroside-positive (GC$^+$) (Fig. 2A and B). Phenylephrine treatment did not significantly change the percentages of neuronal and glial cells (tuj1$^+$, 38.1±3.2%; GFAP$^+$, 28.7±3.1%; and GC$^+$, 6.2±1.0%) in cultures lacking bFGF (Fig. 2A and B). These results indicate that phenylephrine did not affect NPC differentiation induced by bFGF deprivation. We also examined the effect of phenylephrine on neural differentiation of NPCs in cultures containing bFGF and again found no effect on neuronal or glial differentiation (data not shown).

3.3. α_1-adrenoceptor agonists protect NPCs from cell death

It has been reported that activation of α_1-adrenoceptors stimulates DNA synthesis of embryonic NPCs in mixed culture conditions (Pabbathi et al., 1997). Primary NPC cultures prepared from the telencephalon contain a considerable number of neuronal cells (>10%) that also express α_1-adrenoceptors (Papay et al., 2006). To determine whether the previously reported activation of DNA synthesis was indicative of NPC proliferation or proliferation by secondary effect via other cell types contaminating the culture, we re-seeded cultured NPCs from a primary culture to prepare highly purified secondary

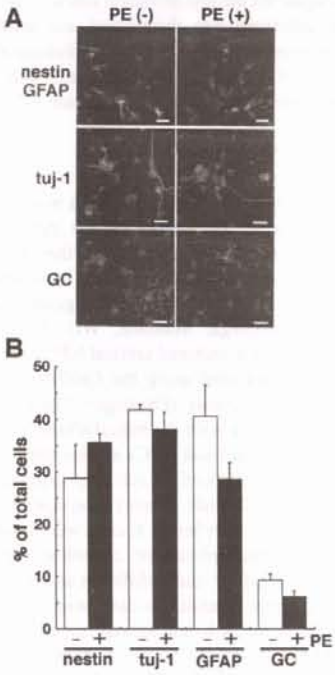

Fig. 2. Effect of the α_1-adrenoceptor agonist phenylephrine on NPC differentiation. (A) Immunofluorescence staining was carried out after 72 h on NPC cultures with or without phenylephrine. Fluorescence microscopic images of cells labeled with anti-nestin (green), anti-GFAP (red), anti-tuj1 (green) and anti-galactocerebroside (green) are shown; nuclei are stained with Hoechst (blue). Scale bar=20 μm. Similar results were obtained in two independent experiments. (B) Secondary cultured NPCs from the E14 mouse telencephalon were maintained *in vitro* for 72 h without or with 10 μM phenylephrine (PE). After 72 h, cells were fixed and immunostained for tuj1, glial fibrillary acidic protein (GFAP), nestin and galactocerebroside (GC). The number of nestin$^+$, tuj1$^+$, GFAP$^+$ and GC$^+$ cells were counted, and the percentages are presented. Nestin was used as a marker for undifferentiated NPCs. No significant differences were observed.

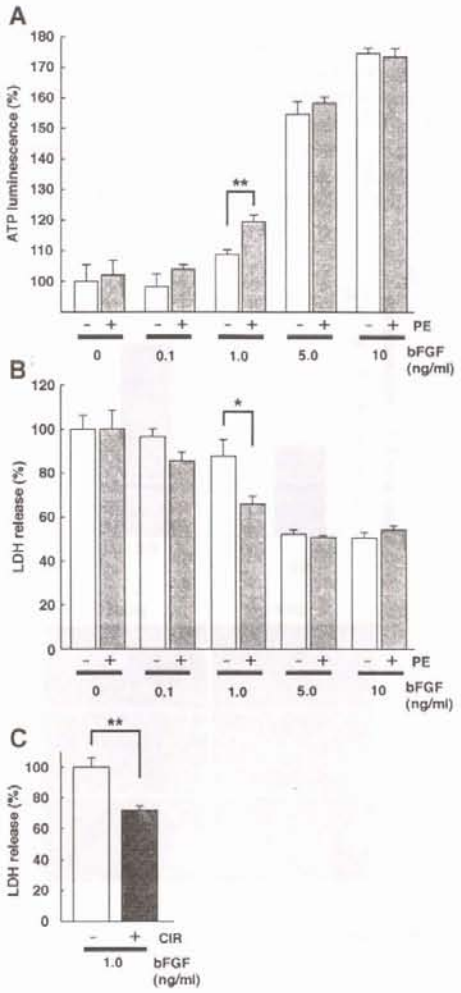

Fig. 3. Effects of α_1-adrenoceptor agonists on the number of cells and cell death of NPCs at various doses of bFGF. Secondary cultured NPCs from the E14 mouse telencephalon were treated without or with 10 μM phenylephrine at different concentrations of bFGF for 24 h. (A) The number of NPCs was examined with an ATP luminescence assay. (B) The viability of NPCs was examined with the LDH release assay. (C) Secondary cultured NPCs from the E14 mouse telencephalon were treated without or with 10 μM cirazoline in 1 ng/ml bFGF for 24 h. Cell survival was assessed by the ATP luminescence assay. Bars represent mean±S.E.M. ($n=4$). Significant differences are indicated by single or double asterisks (*$P<0.05$, **$P<0.01$, Student's t-test).

NPC cultures that contained over 99±0.4% nestin$^+$ undifferentiated NPCs and no more than 0.5% tuj1$^+$ neuronal cells. Using the secondary NPC culture, we examined whether phenylephrine increased the number of NPCs at various doses of bFGF (0~10 ng/ml) using an intracellular ATP luminescence assay (Crouch et al., 1993; Petty et al., 1995). We found that phenylephrine significantly increased the number of NPCs only at a moderate dose (1.0 ng/ml) of bFGF ($P<0.01$; Fig. 3A) and had no significant effect at high doses (5–10 ng/ml), a low dose (0.1 ng/ml) of bFGF, or no bFGF. To determine whether the effect of phenylephrine on NPCs at 1 ng/ml bFGF was due to promotion of cell growth or cell survival, we examine the effect of phenylephrine on cell death using the LDH release assay (Decker and Lohmann-Matthes, 1988), which measures destruction of the plasma membrane. Phenylephrine also significantly decreased LDH release at 1 ng/ml bFGF ($P<0.05$; Fig. 3B), indicating that the difference between ATP luminescence (cell numbers) of phenylephrine-treated and

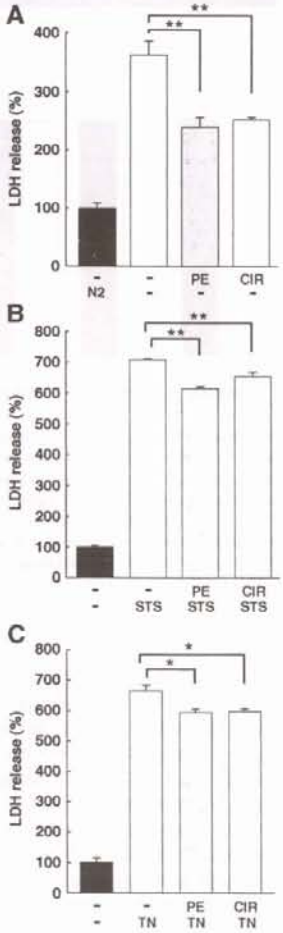

Fig. 4. Phenylephrine and cirazoline promote survival of NPCs under various stress conditions. Secondary cultured NPCs from the E14 mouse telencephalon were incubated in medium lacking N2 (A), 50 nM staurosporine (STS) (B) or 30 ng/ml tunicamycin (TN) (C) in the presence or absence of 10 μM phenylephrine (PE) or 10 μM cirazoline (CIR) for 24 h. Quantification of cell death was performed with the LDH release assay. Bars represent mean±S.E.M. ($n=3\sim5$). Significant differences are indicated by single or double asterisks (*$P<0.05$, **$P<0.01$, Dunnett's test).

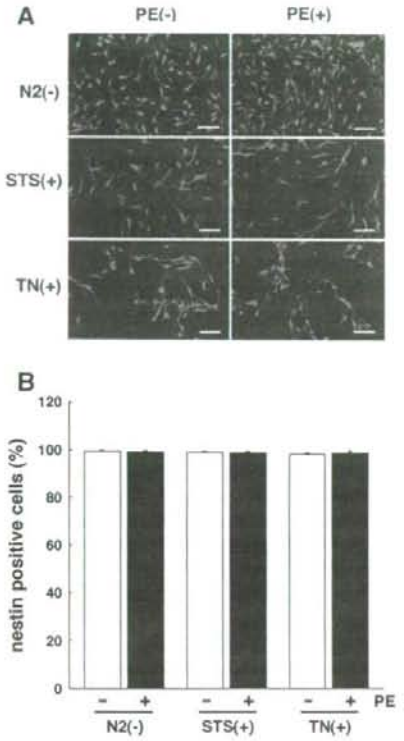

Fig. 5. Effect of phenylephrine on the proportion of nestin-positive cells under various stress conditions. Secondary cultured NPCs were exposed for 24 h to stress conditions without or with 10 μM phenylephrine: N2 deprivation medium, or exposure to 50 nM staurosporine (STS) or 30 ng/ml tunicamycin (TN). After 24 h, the NPCs were fixed and stained with anti-nestin and Hoechst. (A) Fluorescence microscopic images of cells labeled with anti-nestin (green) and Hoechst (blue). Scale bar = 50 μm. (B) The percentages of nestin-positive cells in the cultures were quantified. No significant differences were seen among the groups.

untreated NPCs correlated with the difference in the amount of cell death. These results also indicated that phenylephrine protected NPCs from death during bFGF deprivation-induced stress. Moreover, we confirmed that α_1-adrenoceptor agonists specifically protected NPCs from death using another α_1-adrenoceptor agonist, cirazoline. Cirazoline treatment of NPCs under the same culture conditions resulted in a significant decrease in LDH release ($P<0.01$; Fig. 3C), indicating that α_1-adrenoceptor agonists promote survival of NPCs cultured in 1 ng/ml bFGF. A [^{3}H]thymidine incorporation assay showed that phenylephrine and cirazoline did not induce DNA synthesis of NPCs (data not shown).

3.4. α_1-adrenoceptor agonists prevent NPC death upon exposure to various stresses

To determine the extent to which α_1-adrenoceptor agonists could prevent NPC death, we employed other stress conditions: N2 deprivation, or exposure to 50 nM staurosporine or 30 ng/ml tunicamycin. The results of the LDH release assay for these stress conditions showed that N2 deprivation, staurosporine treatment, and tunicamycin treatment induced LDH release from NPCs (361 ± 24%, 706 ± 5% and 664 ± 21%, respectively, relative to the controls; Fig. 4). However, application of the agonists to the NPC cultures under these stress conditions significantly reduced LDH release (N2 deprivation + phenylephrine, 238 ± 18% $P<0.01$; N2

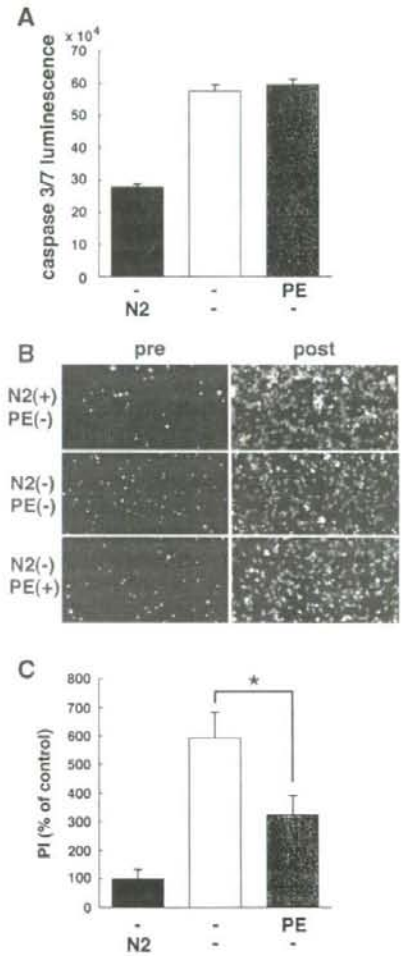

Fig. 6. Phenylephrine does not alter cellular caspase activity but changes propidium iodide penetration into NPCs. Secondary cultured NPCs were incubated without or with 10 μM phenylephrine (PE) under N2 deprivation conditions for 24 h. (A) Caspase-3 and caspase-7 activities in cell lysates were measured by luminometry. (B) Fluorescence microscopy images of dead cells stained with propidium iodide are presented (left). For positive controls, cells were fixed and stained with PI after permeabilization with 0.02% Triton X-100 (right). Scale bar = 100 μm. (C) The intensity of propidium iodide staining was measured by fluorometry. Bars represent mean ± S.E.M. ($n=4$). Significant differences are indicated by an asterisk (*$P<0.05$, Dunnett's test).

deprivation+cirazoline, 251±5% $P<0.01$; staurosporine+phenylephrine, 614±9% $P<0.01$; staurosporine+cirazoline, 654±16% $P<0.01$; and tunicamycin+phenylephrine, 594±13% $P<0.05$; tunicamycin+cirazoline, 597±10% $P<0.05$) (Fig. 4). Under the three stress conditions, the differences in the efficacies of phenylephrine and cirazoline on LDH release did not differ greatly. However, both agonists were most effective against N2 deprivation stress, where phenylephrine and cirazoline reduced LDH release 34% and 31%, respectively, as compared with the unstressed control (Fig. 4A). These data suggest that α_1-adrenoceptor agonists protected NPC death under several different stress conditions but exhibited different efficacies depending on the particular stress.

3.5. α_1-adrenoceptor agonists do not modulate the proportion of nestin-positive NPCs under stress conditions

Phenylephrine did not affect differentiation of NPCs in cultures with or without bFGF (Fig. 1), and the high proportion (over 98%) of nestin-positive cells remained for ~24 h even in 1 ng/ml bFGF (data not shown). The ability of the agonists to prevent cell death in 1 ng/ml bFGF was thus a direct effect on the nestin-positive NPCs and not an artifact due to contaminating cells. We also examined the effects of stress induced by N2 deprivation, 50 nM staurosporine or 30 ng/ml tunicamycin on NPC differentiation to exclude the possibility that the increased cell numbers observed following α_1-adrenoceptor agonist exposure, as measured by ATP production, were derived from the differentiated cells induced by the stresses. The proportion of nestin-positive NPCs was not changed by N2 deprivation, staurosporine-or tunicamycin-induced stress, and treatment of NPCs with phenylephrine or cirazoline under these stress conditions did not decrease the proportions of nestin-positive cells (Fig. 5).

3.6. Phenylephrine inhibits caspase-3/7-independent cell death

Of the three stress conditions tested, α_1-adrenoceptor agonists most effectively suppressed stress caused by N2 deprivation, as measured by LDH release (Figs. 3 and 4). Whereas cell death induced by bFGF deprivation, staurosporine treatment or tunicamycin treatment probably was caused by activation of various death signaling pathways, the stress caused by N2 deprivation mainly induced caspase-3/7-dependent cell death in NPC cultures (Fig. 6). To ascertain whether α_1-adrenoceptor agonists protect against caspase-3/7-dependent cell death, we examined the effects of α_1-adrenoceptor agonists on cellular caspase-3/7 activities. Stress caused by N2 deprivation induced elevated cellular caspase-3 and caspase-7 activities as compared with non-stress conditions (>2 fold; Fig. 6A). However, the elevated activities of caspases were not changed by treatment of NPCs with phenylephrine (Fig. 6A). Despite a lack of modulation of the cellular caspase activity, phenylephrine suppressed propidium iodide penetration into NPC cytoplasm (45.4%; $P<0.05$, as compared with untreated cells deprived of N2) (Fig. 6B and C). These data indicate that α_1-adrenoceptor agonists selectively protect against caspase-3/7-independent death of NPCs exposed to stress.

4. Discussion

In this study, we prepared highly purified embryonic NPCs (>99% nestin$^+$ cells) from the E14 mouse cortex and found that the cortical embryonic NPCs highly express α_{1A}- and α_{1B}-adrenoceptor genes but express the α_{1D}-adrenoceptor gene at low levels. Our pharmacological experiments also revealed that α_1-adrenoceptor agonists are protective against NPC death induced by various stresses without any modification of the cell differentiation state of the NPCs. Moreover we demonstrated that α_1-adrenoceptor agonists reduced NPC death caused by the N2 deprivation stress without modulation of intracellular caspase-3/7 activities.

The α_1-adrenoceptor is expressed in the ventricular zone and subventricular zone of the embryonic rat forebrain (Pabbathi et al., 1997). The ventricular zone of the embryonic cerebral cortex contains both undifferentiated NPCs and differentiated nascent neuronal cells. Our quantitative RT-PCR analysis showed that purified cortical NPCs express α_{1A}- and α_{1B}-adrenoceptor genes at high levels compared with the E14 embryonic telencephalon, suggesting that the undifferentiated NPCs highly expressed the α_{1A}- and α_{1B}-adrenoceptor genes. We could not confirm the expression of α_1-adrenoceptor proteins in NPCs because of low specificity of commercially available antibodies against α_1-adrenoceptor in immunocytochemical experiments with NPCs (data not shown). However, we demonstrated that α_1-adrenoceptor agonists have protective effects against cell death in NPCs, indicating the presence of the α_1-adrenoceptors in NPCs.

The chemical structure of phenylephrine ((*R*)-3-[1-hydroxy-2-(methylamino) ethyl] phenol) differs from that of cirazoline (2-[(2-cyclopropylphenoxy) methyl]-4, 5-dihydro-1H-imidazole). However, both α_1-adrenoceptor agonists had the same effect on NPC death induced by a moderate concentration (1 ng/ml) of bFGF, nutritional deprivation (no N2 supplementation), staurosporine treatment or endoplasmic reticulum stress (tunicamycin treatment), indicating that the effects were specifically mediated by α_1-adrenoceptors. It is well known that cell death can be induced via multiple apoptosis signaling pathways that are specifically activated by different stresses. Although the α_1-adrenoceptor agonists were able to protect NPCs from death induced by the stresses we tested, the molecular mechanism that underlies this broad protection is unknown. However, treatment of NPCs with α_1-adrenoceptor agonists failed to decrease the activities of caspase-3 and caspase-7, which are activated in the apoptosis pathway. Instead, α_1-adrenoceptor agonists reduced propidium iodide incorporation induced by stress caused by N2 deprivation. These data suggest that α_1-adrenoceptor agonists protect against necrotic NPC death but not apoptotic NPC death.

Phenylephrine or cirazoline protects against cell death induced by bFGF deprivation as well as by STS and nutritional deprivation, or treatment with staurosporine or tunicamycin. Niidome et al. (Niidome et al., 2006) showed that NPC death resulting from growth factor deprivation is caused by both caspase-dependent and -independent pathways in concert with oxidative stress, suggesting that α_1-adrenoreceptor agonists may also protect against NPC death induced by oxidative stresses. On the other hand, application of phenylephrine is effective only against cell death induced by 1.0 ng/ml bFGF. Complete

deprivation of growth factors activates multiple cell death pathways, including apoptosis, necrosis and the oxidative cell death pathway, in cultured NPCs (Niidome et al., 2006). Therefore, the application of phenylephrine is unlikely to be effective against NPC death induced by the overlapping activation of multiple death pathways after complete loss of growth factor support.

In a recent study, Hiramoto et al. (2006) reported that the stimulation of α_1-adrenoreceptors by phenylephrine or by L-epinephrine induces the proliferation of NPCs derived from cultured neurospheres. Our data indicate that α_1-adrenoreceptor agonists do not induce proliferation of purified NPCs. It is known that the neurospheres have the 3D organization in which nestin-positive (progenitor) cells surround a large core of differentiated GFAP-positive (glial) and β-tubulin III-positive (neuronal) cells (Campos, 2004). As such, the NPC cultures prepared from neurospheres could also contain glial and neuronal cells. Thus, the difference between these data may have resulted from differences in the NPC preparation methods and from the purity of the nestin-positive NPCs.

Transplantation of neural stem and progenitor cells into patients with intractable neurological diseases is considered an effective strategy for neural regeneration therapy reviewed in Lindvall et al., (2004). Studies on cell transplantation/implantation for CNS disorders have indicated that neural stem cells and progenitor cells have the ability to replace lost neurons and to repair the damaged nervous system (Chu et al., 2004). However, a large proportion of grafted cells is lost due to early necrotic death. Thus, the low rate of graft survival reduces the effectiveness of such therapies (Emgard et al., 2003). Here we demonstrated that α_1-adrenoceptor agonists protect against NPC death (probably necrotic death) induced by various stresses. We also demonstrated that α_1-adrenoceptor agonists with this protective effect did not modify the cell differentiation state of the NPCs. Thus, α_1-adrenoceptor agonists may be useful for the preparation and maintenance of neural stem and progenitor cells for transplantation therapy, as they are likely to increase cell viability without induction of unexpected cell differentiation. Moreover, phenylephrine is a popular and safe drug that is used as a non-prescription decongestant (Chua and Benrimoj, 1988) Therefore, phenylephrine may be easily applied as an additional reagent in the cultivation medium of neural stem and progenitor cells for transplantation therapy.

Acknowledgments

This work was supported in part by Grants-in-Aid for Scientific Research from the Ministry of Health, Labour and Welfare of Japan, Grants-in-Aid for Scientific Research from the Ministry of Education, Culture, Sports, Science and Technology of Japan, the Program for Promotion of Fundamental Studies in Health Sciences of the National Institute of Biomedical Innovation, and a grant from Japan Science and Technology Agency.

References

Aoki, S., Su, Q., Li, H., Nishikawa, K., Ayukawa, K., Hara, Y., Namikawa, K., Kiryu-Seo, S., Kiyama, H., Wada, K., 2002. Identification of an axotomy-induced glycosylated protein, AIGP1, possibly involved in cell death triggered by endoplasmic reticulum-Golgi stress. J. Neurosci. 22, 10751–10760.

Brewer, G.J., Torricelli, J.R., Evege, E.K., Price, P.J., 1993. Optimized survival of hippocampal neurons in B27-supplemented neurobasal, a new serum-free medium combination. J. Neurosci. Res. 35, 567–576.

Bylund, D.B., Regan, J.W., Faber, J.E., Hieble, J.P., Triggle, C.R., Ruffolo Jr., R.R., 1995. Vascular alpha-adrenoceptors: from the gene to the human. Can. J. Physiol. Pharm. 73, 533–543.

Campos, L.S., 2004. Neurospheres: insights into neural stem cell biology. J. Neurosci. Res. 78, 761–769.

Chu, K., Kim, M., Jung, K.H., Jeon, D., Lee, S.T., Kim, J., Jeong, S.W., Kim, S.U., Lee, S.K., Shin, H.S., Roh, J.K., 2004. Human neural stem cell transplantation reduces spontaneous recurrent seizures following pilocarpine-induced status epilepticus in adult rats. Brain Res. 1023, 213–221.

Chua, S.S., Benrimoj, S.I., 1988. Non-prescription sympathomimetic agents and hypertension. Med. Toxicol. Adverse Drug Exp. 3, 387–417.

Crouch, S.P., Kozlowski, R., Slater, K.J., Fletcher, J., 1993. The use of ATP bioluminescence as a measure of cell proliferation and cytotoxicity. J. Immunol. Methods 160, 81–88.

Decker, T., Lohmann-Matthes, M.L., 1988. A quick and simple method for the quantitation of lactate dehydrogenase release in measurements of cellular cytotoxicity and tumor necrosis factor (TNF) activity. J. Immunol. Methods 115, 61–69.

Emgard, M., Hallin, U., Karlsson, J., Bahr, B.A., Brundin, P., Blomgren, K., 2003. Both apoptosis and necrosis occur early after intracerebral grafting of ventral mesencephalic tissue: a role for protease activation. J. Neurochem. 86, 1223–1232.

Fukazawa, N., Ayukawa, K., Nishikawa, K., Ohashi, H., Ichihara, N., Hikawa, Y., Abe, T., Kudo, Y., Kiyama, H., Wada, K., Aoki, S., 2006. Identification and functional characterization of mouse TPO1 as a myelin membrane protein. Brain Res. 1070, 1–14.

Hieble, J.P., Bondinell, W.E., Ruffolo Jr., R.R., 1995. Alpha- and beta-adrenoceptors: from the gene to the clinic. 1. Molecular biology and adrenoceptor subclassification. J. Med. Chem. 38, 3415–3444.

Hiramoto, T., Ihara, Y., Watanabe, Y., 2006. Alpha-1 Adrenergic receptors stimulation induces the proliferation of neural progenitor cells in vitro. Neurosci. Lett. 408, 25–28.

Lidow, M.S., Rakic, P., 1992. Scheduling of monoaminergic neurotransmitter receptor expression in the primate neocortex during postnatal development. Cereb. Cortex 2, 401–416.

Lidow, M.S., Rakic, P., 1994. Unique profiles of the alpha 1-, alpha 2-, and beta-adrenergic receptors in the developing cortical plate and transient embryonic zones of the rhesus monkey. J. Neurosci. 14, 4064–4078.

Lindvall, O., Kokaia, Z., Martinez-Serrano, A., 2004. Stem cell therapy for human neurodegenerative disorders—how to make it work. Nat. Med. (10 Suppl), S42–S50.

Marien, M.R., Colpaert, F.C., Rosenquist, A.C., 2004. Noradrenergic mechanisms in neurodegenerative diseases: a theory. Brain Res. Brain Res. Rev. 45, 38–78.

Murchison, C.F., Zhang, X.Y., Zhang, W.P., Ouyang, M., Lee, A., Thomas, S.A., 2004. A distinct role for norepinephrine in memory retrieval. Cell 117, 131–143.

Niidome, T., Morimoto, N., Iijima, S., Akaike, A., Kihara, T., Sugimoto, H., 2006. Mechanisms of cell death of neural progenitor cells caused by trophic support deprivation. Eur. J. Pharmacol. 548, 1–8.

Pabbathi, V.K., Brennan, H., Muxworthy, A., Gill, L., Holmes, F.E., Vignes, M., Haynes, L.W., 1997. Catecholaminergic regulation of proliferation and survival in rat forebrain paraventricular germinal cells. Brain Res. 760, 22–33.

Papay, R., Gaivin, R., Jha, A., McCune, D.F., McGrath, J.C., Rodrigo, M.C., Simpson, P.C., Doze, V.A., Perez, D.M., 2006. Localization of the mouse alpha1A-adrenergic receptor (AR) in the brain: alpha1AAR is expressed in neurons, GABAergic interneurons, and NG2 oligodendrocyte progenitors. J. Comp. Neurol. 497, 209–222.

Petty, R.D., Sutherland, L.A., Hunter, E.M., Cree, I.A., 1995. Comparison of MTT and ATP-based assays for the measurement of viable cell number. J. Biolumin. Chemilumin. 10, 29–34.

Popovik, E., Haynes, L.W., 2000. Survival and mitogenesis of neuroepithelial cells are influenced by noradrenergic but not cholinergic innervation in cultured embryonic rat neopallium. Brain Res. 853, 227–235.

Sakurai, M., Ayukawa, K., Setsuie, R., Nishikawa, K., Hara, Y., Ohashi, H., Nishimoto, M., Abe, T., Kudo, Y., Sekiguchi, M., Sato, Y., Aoki, S., Noda, M., Wada, K., 2006. Ubiquitin C-terminal hydrolase L1 regulates the morphology of neural progenitor cells and modulates their differentiation. J. Cell Sci. 119, 162–171.

Slotkin, T.A., Windh, R., Whitmore, W.L., Seidler, F.J., 1988. Adrenergic control of DNA synthesis in developing rat brain regions: effects of intracisternal administration of isoproterenol. Brain Res. Bull. 21, 737–740.

Southwick, S.M., Bremner, J.D., Rasmusson, A., Morgan 3rd, C.A., Arnsten, A., Charney, D.S., 1999. Role of norepinephrine in the pathophysiology and treatment of posttraumatic stress disorder. Biol. Psychiatry 46, 1192–1204.

Zhong, H., Minneman, K.P., 1999. Alpha1-adrenoceptor subtypes. Eur. J. Pharmacol. 375, 261–276.

Journal of Neurochemistry, 2007, **102**, 1669–1676 doi:10.1111/j.1471-4159.2007.04805.x

Neurotensin type 2 receptor is involved in fear memory in mice

Rena Yamauchi,*,†,‡,[1] Etsuko Wada,*,‡ Sari Kamichi,* Daisuke Yamada,*,‡ Hiroshi Maeno,*,[2] Mina Delawary,§ Takanobu Nakazawa,§ Tadashi Yamamoto§ and Keiji Wada*,‡

**Department of Degenerative Neurological Diseases, National Institute of Neuroscience, National Center of Neurology and Psychiatry, Kodaira, Tokyo, Japan*

†Japan Society for Promotion of Science, Chiyoda-ku, Tokyo, Japan

‡CREST, Japan Science and Technology Agency, Kawaguchi, Saitama, Japan

§Division of Oncology, Department of Cancer Biology, Institute of Medical Science, University of Tokyo, Tokyo, Japan

Abstract

Neurotensin receptor subtype 2 (Ntsr2) is a levocabastine-sensitive neurotensin receptor expressed diffusely throughout the mouse brain. Previously, we found that Ntsr2-deficient mice have an abnormality in the processing of thermal nociception. In this study, to examine the involvement of Ntsr2 in mouse behavior, we performed a fear-conditioning test in Ntsr2-deficient mice. In the contextual fear-conditioning test, the freezing response was significantly reduced in Ntsr2-deficient mice compared with that of wild-type mice. This reduction was observed from 1 h to 3 weeks after conditioning, and neither shock sensitivity nor locomotor activity was altered in Ntsr2-deficient mice. In addition, we found that Ntsr2 mRNA was predominantly expressed in cultured astrocytes and weakly expressed in cultured neurons derived from mouse brain. The combination of *in situ* hybridization and immunohistochemistry showed that Ntsr2 mRNA was dominantly expressed in glial fibrillary acidic protein positive cells in many brain regions including the hypothalamus, while Ntsr2 gene was co-expressed with neuron-specific microtubule associated protein-2 in limited numbers of cells. These results suggest that Ntsr2 in astrocytes and neurons may have unique function like a modulation of fear memory in the mouse brain.

Keywords: astrocytes, fear memory, neuron, neurotensin, neurotensin receptor subtype 2.

J. Neurochem. (2007) **102**, 1669–1676.

Neurotensin (NT) is a bioactive tridecapeptide first isolated from the bovine hypothalamus, and is widely distributed in the central nervous system and peripheral tissues (Carraway and Leeman 1973). There are three subtypes of neurotensin receptors (NTRs): neurotensin receptor subtype 1 (Ntsr1) (Tanaka *et al.* 1990), neurotensin receptor subtype 2 (Ntsr2) (Mazella *et al.* 1996), and neurotensin receptor subtype 3 (Ntsr3) (Mazella *et al.* 1998). Ntsr1 and Ntsr2 are high- and low-affinity receptors, respectively; both are G-protein coupled receptors (GPCRs) with seven-transmembrane domains. Two forms of Ntsr2, a full-length form and a truncated form, have been isolated from rodent brain, and it is thought that these forms are generated by alternative splicing (Botto *et al.* 1997). In cultured cells isolated from rat brain, expression of the full-length form is observed in astrocytes, whereas mRNA for the truncated form is expressed in cultured neurons (Nouel *et al.* 1997, 1999). Ntsr3 is a NT-binding protein having a single transmembrane

Received February 23, 2007; revised manuscript received May 21, 2007; accepted June 20, 2007.

Address correspondence and reprint requests to Etsuko Wada, Department of Degenerative Neurological Diseases, National Institute of Neuroscience, National Center of Neurology and Psychiatry, Ogawahigashi 4-1-1, Kodaira, Tokyo 187-8502, Japan.
E-mail: wada_e@ncnp.go.jp

[1]The present address of Rena Yamauchi is the Department of Biochemistry, School of Pharmaceutical Sciences, Toho University, Funabashi, Chiba 274-8510, Japan.

[2]The present address of Hiroshi Maeno is the Department of Neuroscience, Case Western Reserve University, School of Medicine, Cleveland, OH 44106-4975, USA.

Abbreviations used: CS, cued fear conditioning; DIG, digoxigenin; DA, dopamine; GFAP, glial fibrillary acidic protein; GPCR, G-protein coupled receptor; IHC, immunohistochemistry; ISH, *in situ* hybridization; MAP2, microtubule associated protein-2; NT, neurotensin; NTR, neurotensin receptor; Ntsr1, neurotensin receptor subtype 1; Ntsr2, neurotensin receptor subtype 2; TSA, tyramide signal amplification; β-LT, β-lactotensin.

structure, but the mechanism of signal transduction through this receptor is not clear (Mazella *et al.* 1998).

Neurotensin is associated with a wide spectrum of biological activities including analgesia, hypothermia, hypotension, stimulation of anterior pituitary hormone release, and cell proliferation (Maeno *et al.* 2004). In addition, NT may be involved in psychiatric disorders and drug abuse (Holsboer 2003). For example, the level of NT in the cerebrospinal fluid is lower in some patients with schizophrenia than in controls. Recently, to better understand the function of the NT/NTR system *in vivo*, Ntsr1- and Ntsr2-deficient mice have been established and characterized (Pettibone *et al.* 2002; Remaury *et al.* 2002; Leonetti *et al.* 2004; Maeno *et al.* 2004). Ntsr1-deficient mice show a small increase in body weight and a higher food intake compared with wild-type control mice (Remaury *et al.* 2002). By contrast, Ntsr2-deficient mice have an abnormality in the processing of thermal nociception (Maeno *et al.* 2004). Centrally administered NT stimulates the hypothalamic–pituitary–adrenal axis in rodents, suggesting that NT can modulate the stress response or other aspects of emotional status (Rowe *et al.* 1995). Recently, we reported an anti-stress effect of the Ntsr2 agonist β-lactotensin (β-LT), using restrained mice in a hole-board test (Yamauchi *et al.* 2006). Mice subjected to acute restraint stress exhibited a decreased number of head-dips and increased head-dip latency compared with non-stressed controls in the hole-board test. However, the prior administration of β-LT improved the behaviors caused by stress. Furthermore by the administration of β-LT, the duration of freezing responses by cued fear conditioning was significantly reduced. These findings indicate that Ntsr2 may have an important role in modulation of the emotional behavior.

In situ hybridization (ISH) and immunohistochemistry (IHC) have been performed; however, the distribution of Ntsr2, particularly at the cellular level, remains unclear. For example, rat Ntsr2 mRNA was expressed in glial fibrillary acidic protein (GFAP)-immunoreactive astrocytes both *in vivo* and *in vitro* (Walker *et al.* 1998; Nouel *et al.* 1999). However, using an N-terminal-specific anti-Ntsr2 antibody, no Ntsr2 immunostaining was observed in astrocytes in adult rat brain (Sarret *et al.* 2003).

In this study, to elucidate the effect of the NT/Ntsr2 system in fear memory, we performed a fear-conditioning test in Ntsr2-deficient mice. Furthermore, we identified the property of cells expressing Ntsr2 mRNA by quantitative RT-PCR and a combination of ISH and IHC.

Materials and methods

Animals

Male Ntsr2-deficient mice and wild-type littermates (3–7 months of age) were used for behavioral studies. Male Ntsr2-deficient mice and wild-type littermates were produced in our laboratory by mating Ntsr2 heterozygous males with Ntsr2 heterozygous females or intercrossing with the same genotype (Ntsr2-deficient male mice × Ntsr2-deficient female mice, and wild-type male mice × wild-type female mice, respectively). All mutant mice used in this study were backcrossed to the C57BL/6J mice at least eight times.

Mice were kept in a temperature- and humidity-controlled room with a 12-h light–dark cycle (lights on at 08:00 hours). Food and water were available *ad libitum*. All behavioral experiments were performed between 11:00 and 16:00 hours during the light cycle. All animal experiments were performed in strict accordance with the guidelines of the National Institutes of Neuroscience, National Center of Neurology and Psychiatry (Japan) and were approved by the Animal Investigation Committee of the Institute.

Fear-conditioning test

Fear-conditioning tests were performed using a computerized fear-conditioning system (O'Hara & Co. Ltd, Tokyo, Japan) as previously described (Yamauchi *et al.* 2006). On the conditioning day, each mouse was placed in the conditioning chamber for 2 min before the onset of a tone (70 dBs, 10 kHz) that lasted for 30 s. A foot shock (0.5 mA) was delivered during the last 2 s of the tone. Mice received the foot shock twice, with a 1 min interval in-between. For contextual fear-conditioning test, freezing behavior was examined for 3 min in the same chamber without the tone or foot shock. Whereas in a novel environment, after the habituation period, the same tone (70 dBs, 10 kHz) used during conditioning was given for cued fear-conditioning (CS) test. Freezing score (%) is presented as the ratio of time during the experiment. For long-term experiment, contextual tests were examined using the same mice continuously at 24 h, and 8, 22, and 43 days, and CS tests continuously at 48 h, and 9, 23, and 44 days after conditioning. Consequently, each mouse was investigated for both contextual and CS test at 0, 1, 3, and 6 weeks after conditioning. For short-term experiment, contextual fear-conditioning test was performed using another group of mice at 1 and 5 h after conditioning.

Spontaneous activity test

Spontaneous activity test was performed using an activity monitoring system (Neuroscience Co., Osaka, Japan) as previously described (Yamada *et al.* 2000). Each mouse was placed in the test chamber and locomotor activity, vertical movements (rearing and leaning on the wall), and stereotypic movements (repeated back and forward movements) were measured for 30 min.

Shock sensitivity test

The shock sensitivity test was performed as previously described (Yamada *et al.* 2003). Individual animals were placed on a floor consisting of parallel stainless steel rods (5 mm diameter with gaps of 10 mm) and covered with a 1 L glass beaker. Six series of six shocks (1 s duration, 20, 40, 60, 80, 100, and 130 μA) were delivered at a 15-s interval through the grid floor. Series of shock were administered in ascending and then descending order of magnitude. The least amount of electricity that causes an animal's hind foot left the floor, shock threshold, was defined as the lowest shock sensitivity (μA). For each mouse, a mean shock threshold value was calculated as the average of the six thresholds recorded in the series.

Glial cell cultures

Astrocyte cultures were prepared from post-natal 1-day-old C57BL/6J mice. The cortex and hippocampus were dissected and mechanically dissociated by trituration. Cell suspensions were plated on 10 cm plates at an approximate density of 5×10^6 cells/plate. Cells were incubated in Hepes-buffered Dulbecco's Modified Eagle's Medium/10% fetal bovine serum for 2 weeks, and half of the medium was replaced twice a week.

Oligodendrocyte cultures (CG4 cells) were kindly provided by Drs K. Ikenaka and A. Espinosa de los Monteros. CG4 cells were incubated in glial-defined medium as described (Yonemasu *et al.* 1998).

Neuron cultures

Neuron cultures were prepared from embryonic day 17 (E17) C57BL/6J mice as previously described (Okabe *et al.* 1998). The cell suspension (about 10^7 cells) was plated on 10 cm-diameter poly-L-lysine-coated dish. Cells were incubated in minimal essential medium containing 2% B-27 supplement and 5% fetal bovine serum for 2 weeks.

SYBR Green-based real-time quantitative RT-PCR

Total RNAs of astrocytes and neurons were treated with RNase-free DNase and reverse transcribed with Superscript II (Invitrogen, Carlsbad, CA, USA). Quantification of Ntsr2 mRNA by real-time PCR quantification system (ABI PRISM 7900HT; Applied Biosystems, Foster City, CA, USA) with SYBR Green PCR Master mix (Applied Biosystems) was performed according to the supplier's protocol. For standardization and quantification, hypoxanthine phosphoribosyltransferase was amplified. The following primer pairs were used: 5′-CCGATGATGGATGGACTGATG-3′ (forward) and 5′-AAGGAGGAAGACACGGCATTG-3′ (reverse) for amplification of Ntsr2; and 5′-GTAATGATCAGTCAACGGGGGAC-3′ (forward) and 5′-CCAGCAAGCTTGCAACCTTAACCA-3′ (reverse) for amplification of hypoxanthine phosphoribosyltransferase.

In situ hybridization with ^{35}S-labeled probe

In situ hybridization using a ^{35}S-labeled probe was performed as described (Maeno *et al.* 2004).

Double staining of Ntsr2 mRNA and either MAP2 or GFAP protein

A combination of ISH for Ntsr2 and IHC was performed using a Ventana Discovery Automated ISH System and a RiboMap Kit (Ventana HX system, Ventana, Tucson, AZ, USA) following the manufacturer's instructions. Paraffin sections fixed with formalin were prepared from mouse brain according to a standard protocol. Paraffin sections were automatically deparaffinized, fixed, and treated with protease.

Digoxigenin (DIG)-labeled anti-sense and sense RNA probes were prepared by *in vitro* transcription of a fragment of mouse Ntsr2 cDNA (nucleotides 1239–1483 of GeneBank accession number NM_008747) in pBluescript II SK (−) using T3 and T7 RNA polymerase, respectively. Quality and concentration of DIG-labeled probes were confirmed using a dot-blot assay.

Sections were hybridized with DIG-labeled anti-sense or sense probes at 69°C for 3 h, at a concentration of 25 ng/slide. After hybridization, sections were incubated with a horseradish peroxydase-conjugated anti-DIG antibody (anti-DIG/horseradish peroxydase, 1 : 500, Dako, Glostrup, Denmark). Signals were then enhanced using a tyramide signal amplification (TSA) system using AmpMap with TSA (Ventana). After incubation with alkaline phosphatase, signals were detected in the presence of nitroblue tetrazolium and 5-bromo-4-chloro-3-indolyl phosphate by a Blue Map Kit (Ventana).

Brain sections labeled for ISH with Ntsr2 anti-sense or sense probes were immunostained. Hybridized sections were treated with citric acid and blocking solution. Sections were then incubated with a mouse monoclonal antibody to GFAP (anti-GFAP, 1 : 400, Chemicon, Temecula, CA, USA) or microtubule associated protein-2 (anti-MAP2, 1 : 25, Chemicon) for 60 min at 37°C. Secondary antibody to mouse IgG, at a dilution of 1 : 500, was applied to the sections, and signals were enhanced using the TSA system. Finally, peroxidase activity was detected using 3,3′-diaminobenzidine.

Statistical analysis

The values are presented as the means ± SEM. Statistical analyses were performed using an unpaired Student's *t*-test or ANOVA (followed by Bonferroni's multiple comparison test). *p*-values < 0.05 were considered statistically significant in all statistical tests.

Results

Contextual and cued fear conditioning

We performed fear-conditioning tests with Ntsr2-deficient and wild-type mice to determine the involvement of Ntsr2 in fear memory. During conditioning, the freezing behavior of Ntsr2-deficient mice was not different from that of wild-type control mice (wild type: 10.7 ± 3.0%, $n = 9$; deficient: 5.0 ± 2.5%, $n = 9$; $p > 0.05$).

In the contextual fear-conditioning test, at 24 h after conditioning, the ratio of freezing (%) was significantly decreased in Ntsr2-deficient mice compared with that in wild-type mice (wild type: 49.8 ± 5.9%, $n = 9$; deficient: 27.7 ± 4.1%, $n = 9$; $p < 0.05$, Fig. 1a). This difference in freezing behavior was still evident at 1, 3, and 6 weeks (all $p < 0.01$) after conditioning. In wild-type mice, freezing responses at 1, 3, and 6 weeks after conditioning were reduced compare to that at 24 h after conditioning but not significant (all $p > 0.05$). In contrast, in Ntsr2-deficient mice, freezing responses at 1, 3, and 6 weeks after conditioning were reduced significantly compare with that at 24 h after conditioning (all $p < 0.05$).

In the CS test, at 48 h after conditioning, increased freezing response was observed at the onset of the tone (CS) as compared with the freezing prior to the tone (pre-CS) in both wild-type (pre-CS: 6.2 ± 3.5%, CS: 22.6 ± 6.2%, $n = 8$; $p < 0.05$) and Ntsr2-deficient (pre-CS: 1.9 ± 1.0%, CS: 32.3 ± 4.3%, $n = 9$; $p < 0.001$) mice. The ratio of freezing in Ntsr2-deficient mice was not different from that

